

Heme Distortion Modulated by Ligand-Protein Interactions in Inducible Nitric Oxide Synthase

David Li¹, Dennis J. Stuehr², Syun-Ru Yeh¹ and Denis L. Rousseau^{1*}

1. Department of Physiology and Biophysics, Albert Einstein College of Medicine of Yeshiva University, Bronx, New York 10461

2. Department of Immunology, Lerner Research Institute, Cleveland Clinic, Cleveland, Ohio 44195

Running title: Heme Distortion in Inducible Nitric Oxide Synthase

Author to whom correspondence should be sent:

Denis L. Rousseau
Phone: (718) 430-4264
Fax: (718) 430-8808
E-mail: rousseau@aecom.yu.edu

ABSTRACT

The catalytic center of nitric oxide synthase (NOS) consists of a thiolate coordinated heme macrocycle, a tetrahydrobiopterin (H4B) cofactor and an L-arginine (L-Arg) / N-hydroxy-L-arginine (NOHA) substrate binding site. To determine how the interplay between the cofactor, the substrates, and the protein matrix housing the heme regulates the enzymatic activity of NOS, the CO, NO, and CN⁻-bound adducts of the oxygenase domain of the inducible isoform of NOS (iNOS_{oxy}) were examined with resonance Raman spectroscopy. The Raman data of the CO-bound ferrous protein demonstrated that the presence of L-Arg causes the Fe-C-O moiety to adopt a bent structure due to an H-bonding interaction whereas H4B binding exerts no effect. Similar behavior was found in the CN⁻-bound ferric protein and in the NO-bound ferrous protein. In contrast, in the NO-bound ferric complexes, the addition of L-Arg alone does not affect the structural properties of the Fe-N-O moiety, but H4B binding forces it to adopt a bent structure, which is further enhanced by the subsequent addition of L-Arg. The differential interactions between the various heme ligands and the protein matrix in response to L-Arg and/or H4B binding is coupled to heme distortions, as reflected by the development of a variety of out-of-plane heme modes in the low frequency Raman spectra. The extent and symmetry of heme deformation, modulated by ligand, substrate and cofactor binding, may provide important control over the catalytic and auto-inhibitory properties of the enzyme.

Abbreviations: H4B: tetrahydrobiopterin; NOHA: N-hydroxy-L-arginine; iNOS, eNOS, nNOS: inducible, endothelial and neuronal nitric oxide synthase, respectively; NOS_{FL} and NOS_{oxy}: the full length polypeptide and the oxygenase domain of nitric oxide synthase, respectively; DTT: dithiothreitol; $\nu_{\text{Fe-CO}}$, $\nu_{\text{C-O}}$ and $\delta_{\text{Fe-C-O}}$: the Fe-CO stretching mode, the C-O stretching mode and the Fe-C-O bending mode of the CO bound heme; $\nu_{\text{Fe-NO}}$ and $\delta_{\text{Fe-N-O}}$: the Fe-NO stretching mode and the Fe-N-O bending mode of the NO bound heme; NSD: Normal-coordinate Structural Decomposition; Doop: total out of plane distortion of the heme macrocycle.

INTRODUCTION

Nitric oxide synthase (NOS) catalyzes the formation of NO from oxygen and L-arginine (L-Arg) via a consecutive two-step reaction by using NADPH as the electron source (1-6). In the first step, L-Arg is hydroxylated to N-hydroxyarginine (NOHA). In the second step, NOHA is oxidized to citrulline and NO. Three major isoforms, iNOS, eNOS and nNOS, have been found in macrophages, endothelial cells and neuronal tissues, respectively. All three NOS isoforms are dimeric. Each subunit of the dimer contains two domains: the reductase domain that binds FMN, FAD and NADPH and an oxygenase domain that contains heme and tetrahydrobiopterin (H4B). The electron transfer from the reductase domain to the oxygenase domain, which is essential for the enzymatic activity, is regulated by binding of a calcium-calmodulin complex. When the calcium-calmodulin complex is present, electrons flow from NADPH through FMN and FAD in one subunit to the oxygenase domain of the other subunit (7). The crystal structures of the oxygenase domains from all three isoforms have been determined. They show that the substrate, L-Arg, binds directly above the heme iron atom, while the cofactor, H4B, binds along the side of the heme. Furthermore, the L-Arg and H4B are linked together through an extended H-bonding network mediated by one of the two propionate groups of the heme (8-11).

The functional role of H4B in NOS remains an enigma. Recent experimental evidence has demonstrated that H4B is involved in electron transfer processes in both steps of the catalysis (12-20). EPR and optical absorption data show that during the hydroxylation of L-Arg, the disappearance of the oxygen-bound heme is kinetically and quantitatively coupled to the formation of NOHA and a H4B radical species (15,20), supporting the scenario that H4B serves as an extra electron source. Using rapid freeze-quench EPR and stopped flow optical absorption measurements, it has been demonstrated that in the second step of the catalytic cycle the H4B radical is first formed and then decayed, suggesting that H4B serves as an electron mediator during the reaction (17). Though recent emphasis has been placed on the catalytic role of H4B, experiments have also given indications that it plays an important structural role. Based on the crystal structures of the oxygenase domain of iNOS (iNOS_{oxy}), Crane et al. concluded that H4B binding resulted in major conformational changes to the protein that are critical for the promotion of subunit assembly into a dimer, the active form of NOS, and the formation of the reductase docking site required for the electron transfer (8). In addition, biochemical studies of various isoforms of NOS, showed that H4B binding introduces significant changes in protein stability, monomer/dimer equilibrium, proteolytic susceptibility, heme-ligand binding and substrate binding properties (21-26). In contrast, based on the crystal structure of the oxygenase domain of eNOS (eNOS_{oxy}), Raman et al. reported that H4B binding does not produce any conformational changes in the protein; and more importantly the dimeric assembly is retained in the absence of H4B (11).

The heme iron is coordinated by four pyrrole nitrogen atoms of the porphyrin ring and a proximal thiolate ligand from a cysteine residue. The Fe-S stretching mode of the proximal bond was identified at 338 cm⁻¹ by Schelvis et al. in the resonance Raman spectrum with near UV excitation (27). The Fe-S stretching frequency is lower than that

in cytochrome P-450s, indicating a weaker Fe-S bond that may be important for the catalytic function of NOS. Based on resonance Raman and optical absorption spectra of NOS, in the absence of L-Arg and H4B, the ferric heme iron is in a six-coordinated low-spin electronic configuration with a water or a DTT molecule coordinated to the distal side of the heme. A six-coordinate low-spin to a five-coordinate high-spin heme transition was observed upon H4B or L-Arg binding, reflecting the exclusion of the sixth ligand, either water or DTT, from the heme iron (28-31). This is similar to the low spin to high spin transition observed in the cytochrome P-450 class of proteins, in which a water molecule bound to the heme iron is displaced upon substrate binding (32). It is believed that substrate binding to P450 interferes with ligand binding to the heme iron due to steric constraint imposed by the substrate that is located directly over the heme iron (33,34). The analogous displacement of water or DTT in NOS induced by L-Arg binding has been attributed to the same origin (35). However, such a steric interaction can not account for the H4B binding induced spin transition, considering the fact that the H4B binding site is on the peripheral side of the heme. The origin for the exclusion of the distal ligand upon H4B binding thus has been an open question.

It has been shown that the NO produced at the end of the catalytic reaction remains in the distal pocket and rebinds to the heme iron, thereby inhibiting the enzyme. Although the crystal structures of the oxygenase domains of the three isoforms of NOS are almost identical, the degree of the auto-inhibition by NO follows the order: nNOS > iNOS > eNOS (36,37). Resonance Raman studies of the three NOS isoforms showed that the frequencies of the $\nu_{\text{Fe-CO}}$ and $\nu_{\text{C-O}}$ modes of CO-bound nNOS were shifted with respect to those of eNOS and iNOS in the presence of L-Arg, plausibly due to a unique binding geometry of L-Arg in nNOS with respect to those in eNOS and iNOS (38). However, ENDOR data of the high-spin ferric ligand-free enzyme showed that the binding geometries of L-Arg or NOHA with respect to the heme iron are essentially the same for eNOS, iNOS and nNOS (39).

Biochemical studies have demonstrated that the catalytic mechanism for the conversion from L-Arg to NOHA is fundamentally different than that from NOHA to citrulline (1,2,40,41). This is supported by the ENDOR data, showing that the hydroxylated nitrogen of NOHA is held 3.8 Å from the Fe, closer than the corresponding guanidino N of L-Arg (4.05 Å) in each of the three isoforms (39). However, Raman data showed that the Fe-C-O related vibrational modes of the ferrous CO-bound nNOS in the presence of L-Arg are essentially identical to that in the presence of L-NOHA. Furthermore, the O-O stretching frequency of the oxy-derivative of nNOS_{oxy} in the presence L-Arg is the same as that in the presence of NOHA (42).

As a first step to reconcile these disparate results, we have examined the influence of L-Arg and/or H4B binding on the ligand-protein interactions in iNOS_{oxy}, by using CO, NO and CN⁻ as structural probes for the ferric and ferrous derivatives of iNOS_{oxy}. We found that heme distortion introduced by L-Arg and/or H4B binding plays an important role in modulating the ligand-protein interactions in iNOS_{oxy}. The possible role of this distortion is discussed in the context of the catalytic function of the enzyme.

MATERIALS and METHODS

L-Arginine, DL-Dithiothreitol (DTT), sodium cyanide, and sodium dithionite were purchased from Sigma (St. Louis, MO). (6R)-5,6,7,8-tetrahydro-L-biopterin was purchased from Alexis Biochemicals (San Diego, CA). The natural abundant gases, N₂, CO, and NO, were obtained from Tech Air (White Plains, NY). The isotopically labeled compounds, ¹²C¹⁸O, K¹³C¹⁴N, K¹²C¹⁵N, K¹³C¹⁵N, and ¹⁵N¹⁶O, were supplied by Icon (Mount Marion, NY).

The oxygenase domain of the inducible nitric oxide synthase (iNOS_{oxy}) was expressed in *Escherichia coli* and purified in the absence of both L-Arg and H4B as previously described (42). The enzyme was kept in EPPS buffer at pH 7.6 in the presence of 1mM DTT. Preparations were stored in liquid nitrogen in buffer containing 10% glycerol. Prior to use, the protein was washed three times with EPPS buffer using a centrifugal filtration unit (Ultrafree-15, Biomax-10K NMWL membrane from Millipore). To generate the L-Arg and/or H4B bound derivatives, L-Arg and H4B were added to the filtered enzyme in 100 and 3-5 times excess with respect to the heme, respectively. The enzyme was then incubated for ~18 hours at 4°C. The binding of L-Arg and H4B was confirmed by monitoring changes in the spin and coordination state of the ferric heme with optical absorption spectroscopy. The protein concentration for each sample was approximately 50 μM.

The samples used for optical absorption and resonance Raman spectroscopic measurements on the NO, CO, and CN⁻ derivatives were first purged with N₂ gas in an anaerobic cell. To form the ferric-NO complexes, 400 μl of 1 atm NO was injected into the cell using a Hamilton (Reno, NV) gas tight syringe. Immediately prior to injection, NO gas was scrubbed by passage through a solution of 10 M NaOH. H4B titrations were performed by injecting different volumes of a N₂ purged 1 mM H4B stock solution into the anaerobic sample prior to NO injection. To form the ferrous-CO complexes, the purged samples were reduced with sodium dithionite and 400 μl of 1 atm CO was injected into the cell. To form the ferric-CN⁻ adducts, sodium cyanide solutions were added to the enzyme to a final concentration of 20 mM under anaerobic conditions. Cyanide adducts were kept in anaerobic conditions to minimize oxidation of H4B, which increased fluorescence of samples. Both H4B and cyanide solutions were purged with N₂ gas prior to injection into an anaerobic cell containing sample.

Optical absorption spectra were taken on a Shimadzu UV2100U spectrophotometer. Resonance Raman spectra were obtained by using 406.7 or 413.1 nm excitation from a Kr ion laser (Spectra Physics, Mountain View, CA) or 441.6 nm excitation from a He-Cd laser (Liconix, Santa Clara, CA). The incident power on the sample was kept under 3 mW and the sample cell was rotated at ~6000 rpm during the spectral acquisition to avoid photo-damage. The scattered laser light was collected and focused onto an entrance slit (100 μm) of a 1.25-m SPEX spectrophotometer (Jobin Yvon, Edison, NJ) and was then detected using a liquid nitrogen cooled CCD camera (Roper Scientific, Princeton, NJ). All the resonance Raman spectra were frequency calibrated by using spectral lines from indene (Sigma, Saint Louis, MO), except that in the 1800-2000 cm⁻¹ spectral region, an

acetone/ferricyanide combination was used instead. Cosmic rays artifacts were removed from the spectra by using a routine in the Winspec spectral acquisition software (Roper Scientific, Princeton, NJ). Intensity references were not added to the samples, so the changes that are detected are all relative to the other modes in the spectra. All measurements were made at room temperature. Data were averaged and accumulated for a total integration time of 30 minutes per spectra for most cases. A longer integration time of 60 minutes was used to improve the signal to noise ratio for the CN adducts and the ν_{C-O} spectral region of the CO adduct.

The non-planarity of the hemes was analyzed by the Normal-Coordinate Structural Decomposition (NSD) program written by J. A. Shelnett and available on his Web site (<http://jasheln.unm.edu>). This program analyzes the heme or porphyrin structure, such as those from the protein data bank, and decomposes any distortions into different symmetry types that may be related directly to vibrational modes. It also gives a mean atomic displacement from the ideal square planar geometry of the porphyrin for the total distortion and for each symmetry type (43).

RESULTS

The optical absorption spectra of various oxidation and ligation states of iNOS_{oxy} are shown in Fig. 1. In the absence of L-Arg and H4B, the Soret transition is located at 420 nm, characteristic of a six-coordinate low spin heme (Fig. 1A). Upon the addition of either L-Arg or H4B, the Soret transition shifts to ~400 nm, due to a partial conversion to a five-coordinated high-spin heme. When L-Arg and H4B are both present, the Soret transition further shifts to 395 nm, indicating a full conversion to the five-coordinated high-spin heme. Binding NO or CN⁻ to the ferric heme iron causes a red-shift of the Soret transition to 439 nm as shown in Fig. 1B, typical for a six-coordinated low-spin ferric heme with a proximal cysteine axial ligand. On the other hand, the Soret transition of the CO-bound ferrous protein is located at 445 nm. In contrast to the ligand-free enzyme, the Soret transitions of the NO, CN⁻ and CO-bound complexes were found to be unaffected by the addition of H4B and/or L-Arg (Data not shown).

Resonance Raman spectroscopy with Soret excitation has been successfully applied to study structural and functional relationships of heme proteins for several decades. The high frequency region (1000–1700 cm⁻¹) of the spectrum is very sensitive to the oxidation and coordination states of the heme groups. In particular, the ν_4 vibrational heme mode in the 1340–1380 cm⁻¹ region is very sensitive to the electron density on the heme macrocycle and hence is a good indicator of the oxidation state of the heme iron. The ν_3 vibrational mode in the 1475–1520 cm⁻¹ region is sensitive to both the coordination and spin state of the heme iron, while the ν_2 vibrational mode in the 1560–1590 cm⁻¹ region is sensitive to the heme spin state. In contrast, in the low frequency region of the spectrum (200–800 cm⁻¹), the specific axial ligands coordinated to the prosthetic heme group can be identified by detecting iron-ligand stretching and/or bending modes. In addition, when the prosthetic heme group is deformed from the planar structure, several heme out-of-plane modes may be strongly enhanced in this region of the spectrum (44,45). The frequencies and intensities of the Raman lines are further modulated by the protein

environment surrounding the heme and, therefore, provide useful structural information for heme proteins.

The ligand-free ferric complex. The high frequency resonance Raman spectra of the ferric derivatives of iNOS_{oxy} are presented in Fig. 2. In the absence of L-Arg and H4B (spectrum a), a typical six-coordinate low spin spectrum was obtained with the ν_4 and ν_3 marker lines present at 1372 and 1500 cm^{-1} . Upon the addition of L-Arg, the ν_3 marker line shifts to 1487 cm^{-1} (Fig. 2 spectrum b), indicating a conversion to a five-coordinate high-spin complex. Although the optical absorption spectrum showed only partial conversion from the six-coordinate low-spin state to the five-coordinate high-spin complex (Fig. 1A), only the high-spin component was detected in the resonance Raman spectrum because the spectral lines from the low-spin species were not enhanced with 406.7 nm excitation. The low frequency region of the spectrum was not examined in this study. Nonetheless, in a study of eNOS, changes in certain low frequency modes were identified upon the addition of L-Arg and were interpreted as an indication of a protein structural change (27).

The ferrous CO-bound complex. The low frequency resonance Raman spectra of the ferrous-CO derivatives of iNOS_{oxy} complexes were obtained in the presence and absence of L-Arg and/or H4B (Fig. 3A). In the absence of L-Arg and H4B, the two lines at 491 and 562 cm^{-1} , as shown in the resonance Raman spectrum (a), were assigned to the Fe-CO stretching ($\nu_{\text{Fe-CO}}$) and Fe-C-O bending ($\delta_{\text{Fe-C-O}}$) modes, respectively, based on the isotope difference spectrum shown in Fig. 3B. In the difference spectrum, all the heme modes are cancelled out and the spectral features remaining in the spectrum are associated only with the vibrational modes involving CO. The split of the 491 cm^{-1} mode in the difference spectrum is a result of structural inhomogeneity of the Fe-CO moiety as reflected by a broad feature in the original $\nu_{\text{Fe-CO}}$ mode. With the same isotope substitution experiment, a C-O stretching mode ($\nu_{\text{C-O}}$) was assigned at 1946 cm^{-1} as shown in Fig. 3C. These CO-related vibrational modes are consistent with the previously reported data on the full-length enzyme and on other isoforms (38,42).

No significant shifts in the frequencies or changes in spectral shapes were detected in the CO-related vibrational modes upon the addition of H4B (Fig. 3, spectra c). In contrast, the addition of L-Arg caused a shift in the frequency of the $\nu_{\text{Fe-CO}}$ mode from 491 to 512 cm^{-1} and the $\delta_{\text{Fe-CO}}$ mode from 562 to 569 cm^{-1} (spectra b). In addition, the ν_{CO} mode shifted from 1946 to 1907 cm^{-1} . All three of the Fe-C-O-related modes sharpened in the presence of L-Arg, indicating a direct interaction between L-Arg and the heme-bound CO. Similar spectra were observed in the presence of both L-Arg and H4B (spectra d). Table I summarizes the $\nu_{\text{Fe-CO}}$, $\delta_{\text{Fe-CO}}$, and ν_{CO} modes of the iNOS_{oxy} complexes examined here, and those reported for the other complexes of NOS. The similarity between the oxygenase domain and the full length enzyme indicates that the reductase domain does not significantly modify the heme environment in the oxygenase domain and, hence, the oxygenase domain serves as a valid model for the native enzyme.

In addition to the changes in the Fe-C-O related vibrational modes, small changes in the heme modes were also observed. Most noticeable is the increase in the intensity of a

heme mode at 693 cm^{-1} upon the addition of H4B and/or L-Arg. The mode is strongest in the presence of both L-Arg and H4B, indicating an additive effect of L-Arg and H4B. An enhancement was also observed at 752 and 803 cm^{-1} upon the addition of L-Arg and/or H4B, suggesting that they are of similar origin. Analogous spectral changes were also observed in the reported data for the iNOS_{oxy} domain and for the full-length enzymes of all three isoforms (38,42), indicating that this effect occurs in all three isoforms.

The ferric NO-bound complex. The high frequency resonance Raman spectrum of the ferric NO-bound protein in the absence of H4B and L-Arg is shown in spectrum (c) of Fig. 2. The ν_4 and ν_3 modes were identified at 1372 and 1500 cm^{-1} , respectively, indicative of a six-coordinate low-spin electronic configuration for the heme iron. The oxidation and coordination state of the ferric NO-bound iNOS_{oxy} are not affected by the addition of L-Arg and/or H4B as evident from the high frequency Raman spectra, which was unchanged from that in spectrum (c) of Fig. 2 (data not shown).

The low frequency resonance Raman spectra ($200\text{--}1000\text{ cm}^{-1}$) of the ferric NO-bound iNOS_{oxy} complexes are shown in Fig. 4A. Spectrum (a) is that of the complex in the absence of L-Arg and H4B. The Fe-NO stretching mode ($\nu_{\text{Fe-NO}}$), identified at 537 cm^{-1} , shifts to 533 cm^{-1} upon isotope substitution of $^{14}\text{N}^{16}\text{O}$ with $^{15}\text{N}^{16}\text{O}$. The $\nu_{\text{Fe-NO}}$ mode is not affected by L-Arg binding as shown in spectrum (b). In contrast, in the presence of H4B, two isotopic sensitive lines were detected at 541 and 550 cm^{-1} for the $^{14}\text{N}^{16}\text{O}$ that merge into a single line at 537 cm^{-1} for the $^{15}\text{N}^{16}\text{O}$ adduct as shown in spectrum (c). Although in the absence of H4B, L-Arg does not affect the heme environment, as no discernable differences were observed in the spectrum upon the addition of L-Arg, in the presence of H4B, L-Arg does affect the ligand-related vibrational modes. Upon the addition of L-Arg, in the presence of H4B, one single isotopic sensitive line was observed at 545 cm^{-1} that shifted to 537 cm^{-1} upon the isotope substitution. The larger isotope shift of 8 cm^{-1} with respect to the 4 cm^{-1} shift found in the absence of L-Arg and H4B, suggests that the 545 cm^{-1} mode originates from a Fe-N-O bending mode ($\delta_{\text{Fe-NO}}$), instead of a stretching mode ($\nu_{\text{Fe-NO}}$). Based on this assignment, we assign the 541 and 550 cm^{-1} lines in spectrum (c) to the $\nu_{\text{Fe-NO}}$ and $\delta_{\text{Fe-NO}}$ modes, respectively.

It is important to note that similar Fe-N-O stretching and bending modes have been reported by Hu and Kincaid for cytochrome P-450 and chloroperoxidase (34,46). The authors assigned the low frequency component to the $\nu_{\text{Fe-NO}}$ mode and the high frequency component to the $\delta_{\text{Fe-NO}}$ mode. Furthermore, it was found that, in P-450, the bending mode was also enhanced in the presence of substrate just as observed here for the iNOS_{oxy} complex. However, the substrate in P450 binds directly on top of the NO and the enhancement of the bending mode is accounted for by a direct steric interaction between the substrate and NO, while the H4B binding site found in the crystal structure of NOS is remote from the distal ligand binding site. To examine if there is a second H4B binding site in the distal side of the heme, we titrated H4B into NO-bound iNOS_{oxy} . We found that the binding of H4B to iNOS_{oxy} is stoichiometric with one H4B per protein molecule thereby excluding the possibility of a second binding site for H4B.

In addition to the changes in the Fe-NO stretching and bending modes, the presence of H4B also caused an increase in the relative intensity of the vibrational modes at 685 and 800 cm^{-1} and the appearance of new lines at 352, 390, 710, 729 and 746 cm^{-1} as shown in spectrum (c) in Fig. 4A. The absence of any shifts in these lines upon isotope substitution with $^{15}\text{N}^{16}\text{O}$ confirms that they are not associated with the ligand moiety; instead, they are assigned to the vibrational modes of the heme as will be discussed later. The addition of L-Arg to the H4B-bound protein complex does not introduce additional changes to these heme modes, in contrast to the changes it brings about in the Fe-N-O related modes.

Table II summarizes the $\nu_{\text{Fe-NO}}$ and $\delta_{\text{Fe-N-O}}$ modes determined in this work, in comparison to those reported for other complexes of NOS. The data indicate that H4B binding causes the Fe-N-O moiety to be bent thereby enhancing the bending mode. In addition, the degree of bending of the Fe-N-O moiety is increased in the presence of both H4B and L-Arg, although L-Arg alone does not affect the structure of the Fe-N-O moiety, suggesting that the H4B binding brings L-Arg closer to the heme iron.

The ferrous NO-bound complex. The resonance Raman spectra of the ferrous-NO iNOS_{oxy} complexes were examined in the presence and absence of L-Arg and/or H4B. Unfortunately, in the absence of L-Arg, the ferrous-NO complex is unstable. It forms a five coordinate NO-bound species in the absence of H4B, and undergoes autooxidation in the presence of H4B, consistent with that reported previously (21,47,48). The resonance Raman spectrum of the NO-bound ferrous derivative in the presence of L-Arg alone is shown as spectrum (a) in Fig. 5. Upon the addition of H4B, a Fe-NO related line at 540 cm^{-1} is shifted to 550 cm^{-1} , indicating that H4B affects the heme-bound ligand in a similar fashion as that observed in the ferric-NO complexes (Fig. 4). The inset above spectrum b in Fig. 5 shows the $^{15}\text{N}^{16}\text{O}$ -coordinated form of the ferrous derivative of iNOS_{oxy} in the presence of both L-Arg and H4B. Based on this frequency (533 cm^{-1}) and the isotopic difference spectrum, shown in spectrum (c), we assign the mode at 550 cm^{-1} to the Fe-NO stretching mode ($\nu_{\text{Fe-NO}}$) due to the isotopic shift of 17 cm^{-1} . The assignment of this mode is consistent with that previously reported for the ferrous-NO derivatives of nNOS as listed in Table III (47,49). It is noteworthy that the isotopic shift for the $\nu_{\text{Fe-NO}}$ mode in this ferrous NO complex is much greater than that observed for the ferric NO adducts. Similar isotopic shifts were reported for the NO adducts of the ferrous hemes of cytochrome P-450 and chloroperoxidase (34,46). It was shown by Hu and Kincaid that the large isotopic shift in the ferrous derivative is a consequence of the bent Fe-N-O geometry and the partial mixing of the stretching mode with some bending character (34). In addition to the changes in the $\nu_{\text{Fe-NO}}$ mode, the 692, 715, 734, 752 and 800 cm^{-1} modes were enhanced upon the addition of H4B. Again, they are assigned to the heme modes as was observed in the ferric NO-bound complexes.

The ferric CN^- -bound complex. The high frequency Raman spectrum of the ferric- CN^- derivative in the absence of L-Arg and H4B is shown in Fig. 2, spectrum (d). The ν_3 mode was found at 1500 cm^{-1} , indicating a six-coordinate low-spin species. The addition of L-Arg and/or H4B did not affect the high frequency resonance Raman spectrum of the

CN⁻-bound derivative, demonstrating that the coordination and spin state remains six-coordinate low-spin in the presence of L-Arg and/or H4B (data not shown).

The low frequency resonance Raman spectrum of ferric-CN⁻ complex in the absence of H4B and L-Arg is shown as spectrum (a) in Fig. 6. The addition of L-Arg brings about new lines in the 400-425 cm⁻¹ spectral region. In the presence of H4B alone, the spectrum is similar to that observed in the absence of L-Arg and H4B. On the other hand, the spectrum obtained in the presence of both L-Arg and H4B is very similar to that with L-Arg alone. Cyanide isotope substitution experiments revealed ligand contributions in the lines at 402 and 425 cm⁻¹. The data did not allow for a clear assignment of these modes due to their dependence on the geometry of the Fe-C-N moiety and the mixing of these modes with other heme vibrational modes, as has been shown in cyanide adducts of P450s (50). In P450s, when the Fe-C-N moiety is linear, the Fe-CN stretching mode is located in the 410 – 425 cm⁻¹ region while it is in the 340 – 360 cm⁻¹ region for a bent structure. Furthermore, the Fe-C-N bending mode is in the 385 – 395 cm⁻¹ region for the linear form and the 420 – 440 cm⁻¹ region for the bent structure. Additional measurements are needed for iNOS_{oxy} to make firm assignments of the Fe-C-N modes. Nonetheless, the data indicate that L-Arg has a significant effect on the structure of the Fe-CN moiety, possibly due to a direct interaction between the substrate and the CN⁻ moiety as was observed in the ferrous-CO complexes in contrast to behavior of the ferric-NO complexes.

In addition to the CN⁻ related modes, heme modes are also changed by the addition of substrate and cofactor. Specifically, the presence of H4B results in a large increase in the relative intensity of the mode at 691 cm⁻¹, and a small enhancement in the mode at 713 cm⁻¹. The presence of L-Arg also induces similar intensity changes although to a slightly lesser degree.

DISCUSSION

Heme distortion induced by L-Arg and/or H4B binding. Based upon the results shown in Figs. 3-6, significant changes are seen in the low frequency region of the Raman spectrum upon the addition of H4B, in addition to the changes in the ligand related modes. Changes in low frequency vibrational modes in the resonance Raman spectrum have been seen in other heme protein systems with distorted hemes. A very clear example is cytochrome *c* (45,51). When cytochrome *c* is unfolded, the porphyrin macrocycle adopts a planar structure with D_{4h} symmetry. However, when it is folded, the tertiary interactions cause the porphyrin to take on a ruffled structure. Consequently, several out-of-plane heme modes become active and the low frequency resonance Raman spectrum displays a much more complicated pattern with respect to that of the unfolded protein. We postulate that the changes in the low frequency Raman spectrum of the iNOS_{oxy} complexes induced by L-Arg and/or H4B binding are a result of a change in the distorted structure of the heme. Many studies have been reported in the past on the effects resulting from loss of planarity in porphyrins (52-57). The distortion of the porphyrin results in changes in the energies of the iron d-orbitals as well as the porphyrin

π -orbitals. As a consequence the electronic properties and redox potentials of a heme protein are changed and the electron transfer rate with its partner protein is altered. The distortion of the heme in the crystal structures of the NOS isoforms was discussed by Raman et al. in 2000 (52). It was reported that the binding of H4B did not alter the degree of non-planarity of the heme in the eNOS structure (11). However, as discussed below, based on more recent crystallographic data the addition of H4B does modify the heme planarity in the NO-bound form of reduced eNOS (58).

The most dramatic changes in the low frequency Raman spectra were observed in the NO derivatives of iNOS_{oxy} induced by H4B binding (Figs. 4 and 5). Since the crystal structures of the NO-bound complexes of iNOS_{oxy} have not been reported, we sought to examine the two structures of the ferrous NO-bound eNOS_{oxy} complexes (1FOO and 1FOP) that are available in the PDB (58). cursory examination of the structures indicates that the distortion of the heme is significantly greater in the presence of H4B than in the absence of H4B, when L-Arg is present, as shown in (a) and (b) in Fig. 7. To quantify the degree of distortion, we applied the normal-coordinate structural decomposition method (NSD) developed by Shelnutz and coworkers (43). In the NSD method, the heme distortion is broken down into low-frequency normal coordinates, including ruffling (B_{1u}), saddling (B_{2u}), doming (A_{2u}), waving (E_g) and pyrrole propelling (A_{1u}) deformations as illustrated in the left panel in Fig. 7. With this method, the mean out-of-plane displacement of the atoms in the heme macrocycle associated with each distortion coordinate can be calculated. It should be noted that the degree of heme distortion in the two subunits of the dimer is somewhat different, presumably due to inter-subunit interactions. For this discussion we use the average value calculated from the two subunits for each complex as listed in Table IV, since in most cases the trend is similar in the two subunits. It is also important to point out that the typical out-of-plane distortion for most heme proteins, such as hemoglobin and myoglobin, is $\sim 0 - 0.7$ Å; and only a few heme protein contain very distorted hemes with a distortion of > 1 Å (43).

We found that, the total out-of-plane distortion (Doop) of the ligand-free ferrous eNOS_{oxy} is 0.97 Å in the presence of L-Arg and in the absence of H4B (1FOL (58) in Table IV). It is decreased to 0.77 Å upon NO binding (1FOO (58)), indicating a decrease in the heme distortion. Further addition of H4B restores the distorted heme, as reflected by the increase of Doop to 1.00 Å (1FOP (58)). These results indicate that the heme distortion is very sensitive to ligand and cofactor binding. They also confirm the increased distortion to the NO-bound heme upon H4B binding as shown in Fig. 7 (a) and (b). It is important to note that the major contribution to the changes in distortion is saddling with a B_{2u} symmetry that decreased from 0.65 Å to 0.42 Å upon the binding of NO, and then increased to 0.68 Å upon the addition of H4B to the NO bound protein (Table IV).

Although NO binding to the ferrous eNOS_{oxy} in the presence of L-Arg alone reduces the degree of heme distortion, CN⁻ binding to the ferric iNOS_{oxy} in the presence of both L-Arg and H4B causes the Doop to increase from 0.83 to 1.08 Å (1NOD (8) vs 1N2N (59)). Furthermore, the major contribution to the changes in distortion is a combination of saddling and doming with B_{2u} and A_{2u} symmetries, respectively, as listed in Table IV. It

is also interesting to note that the B_{2u} out of plane distortion is greatly diminished in a monomeric form of $iNOS_{oxy}$ that does not bind H4B (iNOS (9)), suggesting the B_{2u} distortion may be partially associated with inter-subunit interactions in the dimer, although the presence of imidazole in this structure may have influenced the degree of distortion.

Based on the assignments of the vibrational modes in ferrochelatase, which also exhibits a very distorted heme (44), several of the modes in the resonance Raman spectra of the NO-bound ferric complexes can be tentatively assigned (Fig. 4). In the absence of L-Arg and H4B, shown as the spectrum (a) in Fig. 4, the lines at 344, 676, and 752 cm^{-1} are assigned as ν_6 , ν_7 and ν_{16} , respectively. The weak 685 cm^{-1} mode is assigned to an out-of-plane mode, γ_{15} , with B_{2u} symmetry. The presence of the weak 685 cm^{-1} line, in the spectrum (a) and (b) in Fig. 4 thus suggests that the NO-bound ferric heme is slightly saddled in the absence of H4B. In the presence of H4B the new lines at 352, 710, 729 and 746 cm^{-1} are assigned to the out-of-plane modes, γ_6 , γ_{11} , γ_5 and γ_1 , respectively. The presence of these out-of-plane Raman modes allow for the determination of the symmetry of the distorted heme induced by H4B binding. The γ_6 (352 cm^{-1}) and γ_5 (729 cm^{-1}) modes are both of A_{2u} symmetry and are consistent with a doming type of deformation. On the other hand, the γ_{15} (685 cm^{-1}), γ_{11} (710 cm^{-1}) and γ_1 (746 cm^{-1}) modes have B_{2u} , B_{1u} , and A_{1u} symmetries, respectively, which are consistent with the saddling, ruffling and propeller deformations, respectively. The presence of these out-of-plane modes with differing symmetry types suggest that the heme is distorted along several coordinates. The similarity between the two spectra shown in Fig. 4A (a) and (b) and that between Fig. 4A (c) and (d) suggests that L-Arg binding does not introduce significant distortion to the NO-bound ferric heme. In addition to heme deformation, the enhancement of the 390 cm^{-1} line, which is assigned to a propionate mode, in the spectra (c) and (d), suggests that the orientation of the propionate group with respect to the heme macrocycle is changed upon H4B binding probably due to a direct H-bonding interaction between the propionate and the H4B as indicated in the crystal structures of iNOS.

In the ferrous NO-bound derivative, only the spectra in the presence of L-Arg alone and in the presence of both L-Arg and H4B were obtained because in the absence of L-Arg the protein is not stable. The H4B binding greatly enhances the 692 cm^{-1} line (γ_{15}) with B_{2u} symmetry. It also brings about small increases in the 715 (γ_{11}) and 734 cm^{-1} (γ_5) lines with B_{1u} and A_{2u} symmetries, respectively. These changes suggest a large change in the saddling (B_{2u}) deformation and small changes in the doming (A_{2u}) and ruffling (B_{1u}) deformations, and are consistent with the NSD analysis of the NO-bound ferrous derivative of $eNOS_{oxy}$ in which the addition of H4B in the presence of L-Arg generated a large change in the saddling deformation (0.42 to 0.68 Å) and small changes in the doming and ruffling coordinates (Table IV).

In the CN^- -bound derivative, the major change induced by the addition of H4B is an increase in the 692 cm^{-1} line, which is assigned to the γ_{15} mode with B_{2u} symmetry. Again it indicates an increase in the heme deformation along the saddling coordinate. This is consistent with the NSD analysis in which the largest deformation (0.79 Å) in the CN^- -derivative of $iNOS_{oxy}$ occurs along the saddling coordinate.

The degree of heme distortion in the CO-bound derivative is smaller than that of the other derivatives of iNOS_{oxy} examined in this work. The addition of L-Arg alone induces minute changes to heme distortion as reflected by small enhancement in the 693, 718, 752 and 803 cm⁻¹ modes (Fig. 3, spectrum b). A similar degree of heme distortion was observed upon H4B binding as shown in spectrum (c). The structural effects imposed by L-Arg and H4B binding appear to be additive, hence a larger degree of heme distortion was observed in the presence of both L-Arg and H4B. As in the other derivatives, the largest change is in the 693 cm⁻¹ (γ_{15}) line, thereby suggesting a B_{2u} saddling deformation. The change at 718 cm⁻¹ (γ_{11}) line suggests a small B_{1u} ruffling deformation. In the absence of L-Arg and H4B, none of the heme distortion modes are significant, as shown in Fig. 3 spectrum (a), suggesting that the heme is in a planar geometry. The substrate and cofactor induced heme deformation in iNOS_{oxy} is in sharp contrast to that of the nNOS_{oxy} complex. In the CO derivative of nNOS_{oxy}, two lines at 722 and 773 cm⁻¹ are detected in the absence of the substrate and cofactor (42), which we tentatively assign as the γ_{11} mode (B_{1u}) and the ν_{15} mode (B_{1g}), respectively. The presence of the two modes suggests that, in the absence of substrate and cofactor, the heme in the CO-bound nNOS_{oxy} is ruffled. Substrate and cofactor binding causes the heme to convert to a more planar structure as indicated by the disappearance of the γ_{11} and ν_{15} modes. The opposite behavior in nNOS_{oxy} and iNOS_{oxy} reflects the subtle differences in the structural properties of these two isoforms.

It is noteworthy that the addition of H4B to all the iNOS_{oxy} derivatives examined here caused an increase in the heme deformation along the saddling coordinate as reflected by the increase in the γ_{15} mode. This is consistent with the NSD analysis in which a high degree of saddling deformation is observed in all of the derivatives examined, except that in the monomeric derivative (1NOS (9) in Table IV). Furthermore, due to the differences in the electronic properties of the heme iron and the heme-bound ligand, the degree of heme deformation is in the following order: Fe⁺³-NO > Fe⁺²-NO > Fe⁺³-CN⁻ > Fe⁺²-CO.

Influence of L-Arg and/or H4B on the structural properties of heme-bound ligands.

The presence of L-Arg and/or H4B in iNOS_{oxy} does not only induce heme distortion, it also affects the structural properties of the heme-bound ligands. The stability of an exogenous ligand that coordinates to the sixth position of a heme group depends on the electronic properties of the ligand, the heme iron and the proximal residue, as well as the environment of the distal binding pocket. Strong-field distal ligands, for example CO, NO, CN⁻ or imidazole, typically form stable complexes. On the other hand, weak-field distal ligands, such as water or DTT, form complexes that are much more labile. In some cases, the binding of a weak ligand to heme iron requires the stabilization provided by polar residues in the distal pocket. A well known example is aquo metmyoglobin, in which the heme-bound water is stabilized by a distal histidine residue through a H-bond (60). Mutation of the distal histidine to a nonpolar residue destabilizes the water leading to a five coordinate state. The distal water ligand in metmyoglobin can also be destabilized through the mutation of the proximal histidine ligand to cysteine, due to the alteration in the electronic properties of the proximal ligand (61). In cytochrome *c* peroxidase, it is believed that the imidazolate character of the proximal ligand strengthens

the proximal iron-histidine bond thus pulling the heme iron out of the porphyrin plane and hindering the coordination of water to the heme iron. In most P450 type of proteins, the substrate-free protein is six coordinate with a water bound to the distal site. Upon substrate binding to the distal site, the distal water ligand may be displaced resulting in a five coordinate high spin heme due to unfavorable substrate-ligand steric interactions (62,63). In contrast, in the substrate-free form of chloroperoxidase (PDB: 1CPO (64)), which like P450 has a cysteine proximal ligand, a five coordinate heme was observed although there is a water molecule in the distal pocket that is only 3.3 Å away from the heme iron (64).

The addition of L-Arg to the ferric derivative of NOS brings about a conversion from the six-coordinate low-spin heme to a five-coordinate high-spin heme as demonstrated in Fig. 1, indicating the exclusion of a distal water molecule from the heme iron. In NOS, L-Arg binds directly on top of the ligand binding site; the exclusion of the water is thus attributed to steric hindrance imposed by L-Arg, as that observed in P450-type of proteins. A similar six-coordinate low-spin to five-coordinate high-spin transition was also observed upon H4B binding, despite the fact that H4B does not directly interact with the heme ligand based on crystallographic data (8,10,11). On the basis of the H4B titration experiment reported here, the possibility of a second binding site for H4B in the distal pocket is ruled out. A direct steric constraint to the distal water due to an allosteric structural transition is also excluded because the crystal structure of iNOS shows that in the presence of H4B the heme is domed and the heme iron atom is displaced out of the porphyrin plane in the direction of the proximal thiolate ligand, resulting in a very open distal pocket in (PDB: 2NOD) (8). Although a water molecule is present in the distal pocket in this crystal structure, it is 4.28 Å away from the heme iron atom, too far to form a covalent bond to the iron. We postulate that the H-bond between the H4B and the heme propionate group causes the distortion of the heme that destabilizes the bonding between the distal water and the heme iron atom leading to the five-coordinate structure. In addition, a local hydrophobic environment does not lead to stabilizing a bound water molecule.

In the CO-derivatives of iNOS_{oxy}, binding of L-Arg to iNOS_{oxy} causes the $\nu_{\text{Fe-CO}}$ mode to sharpen and shift to higher frequency, regardless of the presence of H4B (Fig. 3 spectra b and d); in addition, the intensity of the $\delta_{\text{Fe-C-O}}$ bending mode is enhanced significantly. These results can be accounted by a direct interaction between the L-Arg and the heme-bound CO. The sharpening of the $\nu_{\text{Fe-CO}}$ line in the presence of L-Arg suggests a decreased conformational freedom for the Fe-C-O moiety due to the presence of a H-bond between the CO and L-Arg. The shift to higher frequency of the Fe-CO stretching mode and the strengthening of the Fe-C-O bending mode indicates that the interaction with the L-Arg also causes the Fe-C-O moiety to become bent (65). The crystal structures of CO bound NOS complexes are not available, but in the CO-free structures, the terminal nitrogen of the guanidinium group of L-Arg is located ~4Å away from the heme iron, suggesting that the CO ligand can be stabilized by L-Arg through a hydrogen bond. A direct hydrogen bonding interaction between the CO ligand and the L-Arg is supported by FTIR studies of the ferrous-CO derivative of iNOS_{oxy}, showing that a 0.8 cm⁻¹ shift in $\nu_{\text{C-O}}$ when the solvent H₂O was replaced with D₂O (66). The presence of

H4B alone makes negligible changes to the Fe-C-O modes but small changes to the heme modes are seen. The small changes in the out-of-plane heme modes upon the addition of L-Arg or H4B indicate a slight deformation of the heme. Interestingly, addition of H4B to the L-Arg-bound protein does not bring about additional changes to the Fe-C-O moiety while the heme distortion is further enhanced, suggesting that the changes in heme deformation do not affect the H-bonding interactions between the L-Arg and the heme-bound CO when H4B is present.

The CO-bound ferrous heme iron and the NO-bound ferric heme iron are isoelectronic; in addition, both of them typically bind in a preferentially perpendicular orientation with respect to the porphyrin plane. It was thus anticipated that L-Arg would interact strongly with NO in the NO-bound ferric derivative in a similar fashion as that observed in the CO-bound ferrous derivative. To our surprise, L-Arg had absolutely no effect on the spectrum of the NO-bound complex in the absence of H4B. Unfortunately, since there are no changes in the spectrum, we are unable to determine if L-Arg binds in a site too far from the NO-bound heme to interact with the NO or if the L-Arg does not bind at all. In contrast, the binding of H4B alone causes the shift of the $\nu_{\text{Fe-NO}}$ mode and the appearance of the $\delta_{\text{Fe-N-O}}$ mode, indicating that the Fe-N-O moiety adopts a bent conformation. It is important to note that so far there is no reported case in which the bending mode is present when the Fe-N-O assumes a linear structure that is perpendicular to the heme plane. A direct interaction between H4B and the Fe-N-O moiety is excluded because there is no evidence that H4B can bind to the distal pocket of NOS. We postulate that the bent Fe-N-O conformation is a result an electronic effect introduced by heme distortion as evident from the enhancement of the heme out-of-plane modes.

Although we are unsure if L-Arg binds to the ferric NO-bound iNOS_{oxy} in the absence of H4B, the distinct spectrum (c) in Fig. 4 with respect to spectrum (d) demonstrates that L-Arg does bind to the protein in the presence of H4B. Upon the addition of L-Arg to the H4B-bound protein, the $\delta_{\text{Fe-N-O}}$ mode is further enhanced and shifted, although the heme out-of plane modes are unaffected. We postulate that, in the presence of H4B, the tilt angle of the Fe-N-O moiety is further increased upon the addition of L-Arg as a result of a direct steric or H-bonding interaction imposed by L-Arg. Similar changes, although not as dramatic, were observed in cytochrome P-450 upon the addition of substrate (34).

To examine if the difference in ligand-protein interactions in the NO-bound ferric protein and the CO-bound ferrous protein is a result of the differences in the redox state of the heme, we examined CN⁻-bound ferric derivative. It was found that the Fe-C-N moiety is much more sensitive to the binding of L-Arg than H4B, similar to the behavior of the ferrous CO-bound derivatives. Thus, we concluded that the ligand-protein interactions are not solely determined by the redox state of the heme iron. The presence of L-Arg in the distal pocket of ferric CN⁻-bound iNOS_{oxy} causes the Fe-C-N moiety to adopt a bent structure, as reflected by the presence of the new $\nu_{\text{Fe-CN}}$ and $\delta_{\text{Fe-C-N}}$ modes (Fig.6). Although distinct changes to the heme deformation modes are visible, the Fe-C-N associated modes are not affected by the binding of H4B alone. However, the binding of H4B in the presence of L-Arg causes the enhancement of the $\delta_{\text{Fe-C-N}}$ mode with respect to the $\nu_{\text{Fe-C-N}}$ mode, suggesting a more bent structure of the Fe-C-N moiety. This change is

associated with further deformation of the heme as evident by the enhancement of the heme out-of-plane modes (spectrum (d) with respect to spectrum (c) in Fig. 6). The bent structure of the Fe-CN moiety and the distorted heme is confirmed in the crystal structure of the cyanide complex of iNOS_{oxy} (PDB: 1N2N (59)).

In the NO-bound ferrous iNOS_{oxy} derivative (Fig. 5), a significant change in the $\nu_{\text{Fe-NO}}$ mode is also present upon H4B binding in the presence of L-Arg, similar to that observed in the ferric NO-bound derivative (spectrum (b) versus spectrum (d) in Fig. 4), again consistent with the conclusion that the ligand-protein interactions are not determined by the redox state of the heme iron. The change in the $\nu_{\text{Fe-NO}}$ mode is concomitant with a further deformation of the heme as evident by the enhancement of the heme out-of-plane modes in Fig. 5(b) with respect to Fig. 5(a). We postulate that the sensitivity of the $\nu_{\text{Fe-NO}}$ mode to H4B is a result of an electronic effect exerted by the distorted heme similar to that observed in the other derivatives of the iNOS_{oxy} complex studied here.

Implications on NOS Physiology. ENDOR studies of the ferric derivatives of NOS, in the presence of H4B and in the absence of any exogenous ligands, show that the positions of the guanidino nitrogen of L-Arg is 4.1 to 4.2 Å away from the heme iron regardless of the type of isoform examined (39), consistent with the crystallographic data showing that the distance ranges from 4.0 to 4.4 Å in the various isoforms. This is in contrast to the conclusions drawn by Fan et al. that a clear structural difference was found for nNOS versus the other two isoforms in the presence L-Arg and H4B based on the resonance Raman studies of the CO-bound ferrous derivatives (38). In that work, the frequency of the $\nu_{\text{Fe-CO}}$ mode of nNOS was found at 503 cm⁻¹ in the presence of L-Arg, in contrast to the 512 cm⁻¹ found for the other two isoforms as shown in Table I.

To determine if the disagreement between the ENDOR and Raman data is a result of the differences in the oxidation state of the heme iron, we compared the ligand related modes of the NO-bound ferric and ferrous derivatives of iNOS to that of nNOS as listed in Table II and III. It was found that the ligand-related frequencies were essentially the same for iNOS and nNOS regardless of the oxidation states of the heme iron. Since the distal binding site appears to be the same for the NO derivatives of the two isoforms regardless of their redox state, we postulate that the differences seen in ENDOR and Raman data may be a consequence of a distinct heme distortion or proximal bond strength in nNOS with respect to iNOS (and eNOS) in response to CO coordination. Current experiments are planned to distinguish between these possibilities.

It has been shown that the NO generated from NOS plays an important role in regulating its enzymatic activity by forming a self-inhibitory complex with the heme iron and by influencing the stability of the dimeric interaction (67). At the completion of the catalytic cycle, the NO that is produced in the distal pocket binds geminately to the ferric heme and thereby inhibits the enzyme. Santolini, et al demonstrated that the degree of self-inhibition by NO depends on the following factors: (1) the off-rate of NO from the ferric heme, (2) the ease of reduction of the ferric NO-bound form to the ferrous derivative, and (3) the ease of autooxidation from the ferrous form back to the ferric form (37). Due to isoform specific rates, the degree of self-inhibition differs substantially from one

isoform to the other, ranging from 70-90% in nNOS, to 25% in iNOS and to a negligible amount in eNOS (36). Whether or not NO binding leads to an extensive inhibition strongly depends on the reduction rate of the NO-bound ferric protein to the ferrous derivative in which the NO off-rate is much slower. Here, we found that the ferrous NO-bound complex of iNOS_{oxy} was not stable without L-Arg. In the absence of both L-Arg and H4B, it converts to a five coordinate species. In the presence of H4B alone, it spontaneously auto-oxidizes to the ferric protein. In contrast, the auto-oxidation rate of NO-bound ferrous derivatives of nNOS in the presence of H4B alone is much slower [14, 32, 33]. The higher auto-oxidation rate of iNOS_{oxy} with respect to nNOS, in the presence of H4B alone, may be an important factor that accounts for the lower degree of self-inhibition by NO in iNOS during the enzymatic turnover, since at the end of the catalytic cycle the L-Arg is totally consumed.

In heme proteins with planar heme macrocycles, the reduction of the NO-bound ferric form to the ferrous form happens very rapidly and the NO off-rate from the ferrous protein is extremely slow due to the high stability of the reduced state. In those proteins in which NO delivery is physiologically important, such as nitrophorins, the reduction must be inhibited and this is achieved through heme distortion. Nitrophorins are a family of proteins present in blood sucking insects that release NO to bring about vasodilation and reduction of blood coagulation (68). It was found that the heme in nitrophorin-4 is highly ruffled and the NO is bent despite the fact that there are no residues in the distal pocket that can directly interact with the NO. Typically, the low spin configuration of the ferric iron is $(d_{xy})^2(d_{xz},d_{yz})^3$. However, as pointed out by Walker and collaborators, ruffling of the heme in nitrophorin-4 is associated with a change in the electronic structure to $(d_{xz},d_{yz})^4(d_{xy})^1$ as the unpaired electron in the d_{xy} orbital can not mix with the porphyrin π -system if the heme is planar, whereas upon ruffling of the heme, the π -orbitals of the porphyrin have in-plane components that can overlap with the d_{xy} orbital (69). This allows the half-filled d_{xy} orbital of the heme iron to accept additional electron density from the porphyrin π -orbitals in the ferric oxidation state. This additional electron density in the d_{xy} orbital raises the barrier for the reduction of the iron since in the ferrous oxidation state the d_{xy} orbital is filled by the electrons originating from the iron. As a consequence, the heme iron becomes harder to be reduced.

We postulate that the heme distortion observed in this work serves to regulate the auto-inhibition by making the reduction of the NO-bound heme unfavorable in a similar fashion as that observed in nitrophorins. Moreover, possible differences between the rates of reduction in the isoforms may be a consequence of variations in the heme distortion. In addition to reducing the auto-inhibition when H4B is present, control of the heme distortion may also provide an addition safety control for the living cells when H4B is not available. In this case the distortion is reduced and the enzyme becomes locked in a five-coordinate NO-bound ferrous complex. This may serve to prevent the formation and release of reactive oxygen species which could have deleterious effects on the cells since oxygen exposure to the five-coordinate NO-bound ferrous complex will bring about the formation of nitrate and a ferric heme, which is not harmful to the cell.

The ligand-substrate interactions reported here for the various ligation and oxidation states of iNOS_{oxy} also demonstrate the flexibility of the distal pocket. For example, in the absence of H4B, the L-Arg interacted with the CO in the ferrous CO complex and the cyanide in the ferric cyanide complex but not the NO in the ferric NO complex. As each of these ligands typically binds in a preferentially linear conformation, the distinctive ligand-substrate interaction in the NO derivative demonstrate that there is considerable conformational flexibility in the substrate binding site. Physiologically, NOS first converts L-Arg to NOHA and then from NOHA to L-citrulline. It is well established that the catalytic mechanisms are very different for the two steps of the reaction, although both involve the activation of heme-bound dioxygen and the insertion of oxygen into the substrates. In addition, the citrulline product has to be released and not block the substrate binding site. To carry out the two mechanistically distinct reaction steps and release the citrulline, it is important for the enzyme to adopt different conformations in the heme pocket in response to substrate binding. This structural flexibility observed here may serve to ensure the correct substrate stereochemistry required for the differential reactivity for the two reaction steps. Furthermore, the data reported here show that changes in the electrostatic interactions of the heme-bound ligand have an influence on the substrate positioning. During catalysis as the oxygen goes from its initial electronic structure upon binding to peroxo or ferryl activated complexes, changes in the substrate stereochemistry may be induced by these differences in the oxygen electronic configuration. Thus, substrate binding flexibility may serve to allow for optimization of the substrate during various steps of the catalytic process.

In summary, the data reported here provide a view of the molecular picture underlying NO production reaction in NOS. We show that interactions between the various heme ligands and the protein matrix in response to L-Arg and/or H4B binding are coupled to differing degrees of heme distortion. The heme distortion affects the electronic as well as the structural properties of the heme-bound ligand that may have an important influence on the substrate positioning as well as distinct oxygen chemistry required for the two catalytic steps in NOS. This novel heme distortion in NOS is also very important for the regulation of the NO auto-inhibition to suit the individual physiological needs for each isoform of NOS.

Acknowledgement. We thank Dr. Manon Couture of Laval University of several helpful discussions during the initiation of this project, Dr. John Shelnett of Sandia National Laboratories for help with the NSD analysis and Dr. F. Ann Walker of the University of Arizona. This work was supported by National Institutes of Health Grants CA53914 and GM51491 (to D. J. S.), HL65465 (to S.-R.Y.) and GM54806 (to D.L.R.). D. L. is supported by the Medical Scientist Training Program (GM07288) and the Molecular Biophysics Training Grant (GM08572) at Albert Einstein College of Medicine.

REFERENCES

1. Stuehr, D. J. (1999) *Biochim Biophys Acta* **1411**, 217-230
2. Alderton, W. K., Cooper, C. E., and Knowles, R. G. (2001) *Biochem J* **357**, 593-615
3. Masters, B. S., McMillan, K., Sheta, E. A., Nishimura, J. S., Roman, L. J., and Martasek, P. (1996) *FASEB J* **10**, 552-558
4. Mayer, B., and Andrew, P. (1998) *Naunyn Schmiedeberg's Arch Pharmacol* **358**, 127-133
5. Xie, Q. W., Cho, H., Kashiwabara, Y., Baum, M., Weidner, J. R., Elliston, K., Mumford, R., and Nathan, C. (1994) *J Biol Chem* **269**, 28500-28505
6. Marletta, M. A. (1993) *Adv Exp Med Biol* **338**, 281-284
7. Siddhanta, U., Presta, A., Fan, B., Wolan, D., Rousseau, D. L., and Stuehr, D. J. (1998) *J Biol Chem* **273**, 18950-18958
8. Crane, B. R., Arvai, A. S., Ghosh, D. K., Wu, C., Getzoff, E. D., Stuehr, D. J., and Tainer, J. A. (1998) *Science* **279**, 2121-2126
9. Crane, B. R., Arvai, A. S., Gachhui, R., Wu, C., Ghosh, D. K., Getzoff, E. D., Stuehr, D. J., and Tainer, J. A. (1997) *Science* **278**, 425-431
10. Li, H., Raman, C. S., Glaser, C. B., Blasko, E., Young, T. A., Parkinson, J. F., Whitlow, M., and Poulos, T. L. (1999) *J Biol Chem* **274**, 21276-21284
11. Raman, C. S., Li, H., Martasek, P., Kral, V., Masters, B. S., and Poulos, T. L. (1998) *Cell* **95**, 939-950
12. Wei, C. C., Crane, B. R., and Stuehr, D. J. (2003) *Chem Rev* **103**, 2365-2383
13. Werner, E. R., Gorren, A. C., Heller, R., Werner-Felmayer, G., and Mayer, B. (2003) *Exp Biol Med (Maywood)* **228**, 1291-1302
14. Gorren, A. C., and Mayer, B. (2002) *Curr Drug Metab* **3**, 133-157
15. Wei, C. C., Wang, Z. Q., Meade, A. L., McDonald, J. F., and Stuehr, D. J. (2002) *J Inorg Biochem* **91**, 618-624
16. Hurshman, A. R., Krebs, C., Edmondson, D. E., and Marletta, M. A. (2003) *Biochemistry* **42**, 13287-13303
17. Wei, C. C., Wang, Z. Q., Hemann, C., Hille, R., and Stuehr, D. J. (2003) *J Biol Chem* **278**, 46668-46673
18. Wei, C. C., Wang, Z. Q., Arvai, A. S., Hemann, C., Hille, R., Getzoff, E. D., and Stuehr, D. J. (2003) *Biochemistry* **42**, 1969-1977
19. Hurshman, A. R., and Marletta, M. A. (2002) *Biochemistry* **41**, 3439-3456
20. Hurshman, A. R., Krebs, C., Edmondson, D. E., Huynh, B. H., and Marletta, M. A. (1999) *Biochemistry* **38**, 15689-15696
21. Abu-Soud, H. M., Wu, C., Ghosh, D. K., and Stuehr, D. J. (1998) *Biochemistry* **37**, 3777-3786
22. Berka, V., and Tsai, A. L. (2000) *Biochemistry* **39**, 9373-9383
23. Scheele, J. S., Kharitonov, V. G., Martasek, P., Roman, L. J., Sharma, V. S., Masters, B. S., and Magde, D. (1997) *J Biol Chem* **272**, 12523-12528
24. Sato, H., Nomura, S., Sagami, I., Ito, O., Daff, S., and Shimizu, T. (1998) *FEBS Lett* **430**, 377-380
25. Ghosh, D. K., Wu, C., Pitters, E., Moloney, M., Werner, E. R., Mayer, B., and Stuehr, D. J. (1997) *Biochemistry* **36**, 10609-10619

26. Abu-Soud, H. M., Loftus, M., and Stuehr, D. J. (1995) *Biochemistry* **34**, 11167-11175
27. Schelvis, J. P., Berka, V., Babcock, G. T., and Tsai, A. L. (2002) *Biochemistry* **41**, 5695-5701
28. Wang, J., Stuehr, D. J., Ikeda-Saito, M., and Rousseau, D. L. (1993) *J Biol Chem* **268**, 22255-22258
29. Wu, C., Zhang, J., Abu-Soud, H., Ghosh, D. K., and Stuehr, D. J. (1996) *Biochem Biophys Res Commun* **222**, 439-444
30. Martasek, P., Liu, Q., Liu, J., Roman, L. J., Gross, S. S., Sessa, W. C., and Masters, B. S. (1996) *Biochem Biophys Res Commun* **219**, 359-365
31. Roman, L. J., Sheta, E. A., Martasek, P., Gross, S. S., Liu, Q., and Masters, B. S. (1995) *Proc Natl Acad Sci U S A* **92**, 8428-8432
32. McMillan, K., and Masters, B. S. (1993) *Biochemistry* **32**, 9875-9880
33. Poulos, T. L., and Raag, R. (1992) *FASEB J* **6**, 674-679
34. Hu, S., and Kincaid, J. R. (1991) *J Am Chem Soc* **113**, 2843-2850
35. Abu-Soud, H. M., Wang, J., Rousseau, D. L., and Stuehr, D. J. (1999) *Biochemistry* **38**, 12446-12451
36. Abu-Soud, H. M., Ichimori, K., Nakazawa, H., and Stuehr, D. J. (2001) *Biochemistry* **40**, 6876-6881
37. Santolini, J., Meade, A. L., and Stuehr, D. J. (2001) *J Biol Chem* **276**, 48887-48898
38. Fan, B., Wang, J., Stuehr, D. J., and Rousseau, D. L. (1997) *Biochemistry* **36**, 12660-12665
39. Tierney, D. L., Huang, H., Martasek, P., Roman, L. J., Silverman, R. B., Masters, B. S., and Hoffman, B. M. (2000) *J Am Chem Soc* **122**, 5405-5406
40. Marletta, M. A. (1993) *J Biol Chem* **268**, 12231-12234
41. Korth, H. G., Sustmann, R., Thater, C., Butler, A. R., and Ingold, K. U. (1994) *J Biol Chem* **269**, 17776-17779
42. Couture, M., Stuehr, D. J., and Rousseau, D. L. (2000) *J Biol Chem* **275**, 3201-3205
43. Shelnutz, J. A. (2000) in *The Porphyrin Handbook* (Kadish, K. M., K. M. Smith, and Guilard, R., eds) Vol. 7, pp. 168-223, Academic Press, New York
44. Blackwood, M. E., Jr., Rush, T. S., 3rd, Romesberg, F., Schultz, P. G., and Spiro, T. G. (1998) *Biochemistry* **37**, 779-782
45. Yeh, S. R., Takahashi, S., Fan, B., and Rousseau, D. L. (1997) *Nat Struct Biol* **4**, 51-56
46. Hu, S., and Kincaid, J. R. (1993) *J Biol Chem* **268**, 6189-6193
47. Couture, M., Adak, S., Stuehr, D. J., and Rousseau, D. L. (2001) *J Biol Chem* **276**, 38280-38288
48. Wang, J., Rousseau, D. L., Abu-Soud, H. M., and Stuehr, D. J. (1994) *Proc Natl Acad Sci U S A* **91**, 10512-10516
49. Abu-Soud, H. M., Wang, J., Rousseau, D. L., Fukuto, J. M., Ignarro, L. J., and Stuehr, D. J. (1995) *J Biol Chem* **270**, 22997-23006
50. Deng, T., Macdonald, I. D., Simianu, M. C., Sykora, M., Kincaid, J. R., and Sligar, S. G. (2001) *J Am Chem Soc* **123**, 269-278
51. Jordan, T., Eads, J. C., and Spiro, T. G. (1995) *Protein Sci* **4**, 716-728

52. Raman, C. S., Martasek, P., and Masters, B. S. (2000) in *The Porphyrin Handbook* (Kadish, K. M., K. M. Smith, and Guillard, R., eds) Vol. 4, pp. 293-339, Academic Press, New York
53. Renner, M. W., Barkigia, K. M., Zhang, Y., Medforth, C. J., Smith, K. M., and Fajer, J. (1994) *J Am Chem Soc* **116**, 8582-8592
54. Barkigia, K. M., Renner, M. W., Furenlid, L. R., Medforth, C. J., Smith, K. M., and Fajer, J. (1993) *J Am Chem Soc* **115**, 3627-3635
55. Barkigia, K. M., Berber, M. D., Fajer, J., Medforth, C. J., Renner, M. W., and Smith, K. M. (1990) *J Am Chem Soc* **112**, 8851-8857
56. Barkigia, K. M., Chantranupong, L., Smith, K. M., and Fajer, J. (1988) *J Am Chem Soc* **110**, 7566-7567
57. Fukuzumi, S., Nakanishi, I., Barbe, J.-M., Guillard, R., Caemelbecke, E. V., Guo, N., and Kadish, K. M. (1999) *Angewandte Chemie International Edition* **38**, 964-966
58. Li, H., Raman, C. S., Martasek, P., Masters, B. S., and Poulos, T. L. (2001) *Biochemistry* **40**, 5399-5406
59. Fedorov, R., Ghosh, D. K., and Schlichting, I. (2003) *Arch Biochem Biophys* **409**, 25-31
60. Quillin, M. L., Arduini, R. M., Olson, J. S., and Phillips, G. N., Jr. (1993) *J Mol Biol* **234**, 140-155
61. Adachi, S., Nagano, S., Ishimori, K., Watanabe, Y., Morishima, I., Egawa, T., Kitagawa, T., and Makino, R. (1993) *Biochemistry* **32**, 241-252
62. Haines, D. C., Tomchick, D. R., Machius, M., and Peterson, J. A. (2001) *Biochemistry* **40**, 13456-13465
63. Tsubaki, M., Ichikawa, Y., Fujimoto, Y., Yu, N. T., and Hori, H. (1990) *Biochemistry* **29**, 8805-8812
64. Sundaramoorthy, M., Ternner, J., and Poulos, T. L. (1995) *Structure* **3**, 1367-1377
65. Yu, N.-T., and Kerr, E. A. (1987) in *Biological Applications of Raman Spectroscopy* (Spiro, T. G., ed) Vol. 3, pp. 39-96, 3 vols., John Wiley & Sons, New York
66. Jung, C., Stuehr, D. J., and Ghosh, D. K. (2000) *Biochemistry* **39**, 10163-10171
67. Chen, Y., Panda, K., and Stuehr, D. J. (2002) *Biochemistry* **41**, 4618-4625
68. Valenzuela, J. G., Walker, F. A., and Ribeiro, J. M. (1995) *J Exp Biol* **198** (Pt 7), 1519-1526
69. Roberts, S. A., Weichsel, A., Qiu, Y., Shelnut, J. A., Walker, F. A., and Montfort, W. R. (2001) *Biochemistry* **40**, 11327-11337
70. Wang, J., Stuehr, D. J., and Rousseau, D. L. (1997) *Biochemistry* **36**, 4595-4606

FIGURE CAPTIONS

Figure 1. Optical absorption spectra of $iNOS_{oxy}$. Panel A: Spectra of the ferric form of $iNOS_{oxy}$. (a) $-Arg/-H4B$, (b) $+Arg/-H4B$, (c) $-Arg/+H4B$, (d) $+Arg/+H4B$. Panel B: Spectra of ligand-bound complexes of $iNOS_{oxy}$ all measured in the absence of L-Arg and H4B. (a) Ferrous-CO complex, (b) ferric-NO complex, (c) ferric- CN^- complex.

Figure 2. Resonance Raman spectra of the ferric forms of $iNOS_{oxy}$. (a) Exogenous ligand-free ferric form ($-Arg/-H4B$), (b) Exogenous ligand-free ferric form ($+Arg/-H4B$), (c) ferric-NO complex ($-Arg/-H4B$), (d) ferric- CN^- complex ($-Arg/-H4B$). The excitation wavelengths for the spectra (a) and (b) were 413 and 406 nm, respectively, and that for spectra (c) and (d) was 442 nm. The lines marked with an asterisk (*) denote the plasma lines from the laser.

Figure 3. Resonance Raman spectra of the ferrous-CO-bound complexes of $iNOS_{oxy}$. Panel A: Spectra of the complexes in the presence and/or absence of L-Arg and H4B. (a) $-Arg/-H4B$, (b) $+Arg/-H4B$, (c) $-Arg/+H4B$, (d) $+Arg/+H4B$. Panel B: Isotopic difference spectrum ($^{12}C^{16}O - ^{12}C^{18}O$) in the ν_{Fe-CO} spectral region. (a) $-Arg/-H4B$, (b) $+Arg/-H4B$, (c) $-Arg/+H4B$, (d) $+Arg/+H4B$. Panel C: Isotope difference spectrum ($^{12}C^{16}O - ^{12}C^{18}O$) in the ν_{C-O} spectral region. (a) $-Arg/-H4B$, (b) $+Arg/-H4B$, (c) $-Arg/+H4B$, (d) $+Arg/+H4B$. All spectra were taken with an excitation wavelength of 442 nm.

Figure 4. Panel A: Resonance Raman spectra of the NO-bound ferric complexes of $iNOS_{oxy}$ in the presence and/or absence of L-Arg and H4B. The isotope sensitive peaks determined from the $^{15}N^{16}O$ -bound ferric- $iNOS_{oxy}$ complexes are shown in the inset above their corresponding peaks associated with the natural abundance species. (a) $-Arg/-H4B$, (b) $+Arg/-H4B$, (c) $-Arg/+H4B$, (d) $+Arg/+H4B$. Panel B: Isotope difference spectrum ($^{14}N^{16}O - ^{15}N^{16}O$). (a) $-Arg/-H4B$, (b) $+Arg/-H4B$, (c) $-Arg/+H4B$, (d) $+Arg/+H4B$. All spectra were taken with an excitation wavelength at 442 nm.

Figure 5. Resonance Raman spectra of the ferrous-NO complexes of $iNOS_{oxy}$. (a) $^{14}N^{16}O$ ($+Arg/-H4B$), (b) $^{14}N^{16}O$ ($+Arg/+H4B$). The inset shows the isotope ($^{15}N^{16}O$) sensitive peak in the presence of both L-Arg and H4B, (c) $^{14}N^{16}O - ^{15}N^{16}O$ difference spectrum for the $+Arg/+H4B$ samples. All spectra were taken with an excitation wavelength of 442 nm.

Fig. 6. Resonance Raman spectra of the CN^- -bound ferric complexes of $iNOS_{oxy}$ in the presence and/or absence of L-Arg and H4B. (a) $-Arg/-H4B$, (b) $+Arg/-H4B$, (c) $-Arg/+H4B$, (d) $+Arg/+H4B$. All spectra were taken with an excitation wavelength of 442 nm.

Fig. 7. Heme distortion. Left: Symmetry types for non-planar distortion of the porphyrin macrocycle used for the normal coordinate structural decomposition (NSD) from Shelnett et al. (43). sad: saddling, ruf: ruffling, dom: doming, wav: waving, pro: propellering. Right: Total mean out-of-plane heme distortion for several forms of NOS_{oxy} obtained

from an NSD analysis of the reported crystal structures. For clarity the methane bridge carbon atoms were deleted for the structures. (a) NO-bound ferrous eNOS_{oxy} in the presence of L-Arg but the absence of H4B. (b) NO-bound ferrous eNOS_{oxy} in the presence of L-Arg and H4B. The addition of H4B causes an increase in the heme distortion from 0.77 to 1.00 Å. (c) CN⁻-bound ferric iNOS_{oxy} in the presence of L-Arg and H4B. (d) Ferric iNOS_{oxy} in the presence of L-Arg and H4B.

Table I: Listing of the $\nu_{\text{Fe-CO}}$, $\delta_{\text{Fe-CO}}$, and ν_{CO} modes of the CO-bound ferrous complexes of iNOS_{oxy}, full length iNOS (iNOS_{FL}), nNOS_{oxy}, full length nNOS (nNOS_{FL}), and full length eNOS (eNOS_{FL})

Complex (Fe ⁺² -CO)	$\nu_{\text{Fe-CO}}$ (cm ⁻¹)	$\delta_{\text{Fe-CO}}$ (cm ⁻¹)	ν_{CO} (cm ⁻¹)	Ref
iNOS _{oxy}	491 (Broad)	562	1946	This work.
iNOS _{oxy} + L-Arg	512	569	1907	This work.
iNOS _{oxy} + H4B	490 (Broad)	562	1944	This work.
iNOS _{oxy} + L-Arg + H4B	512	569	1905	This work.
iNOS _{FL} + H4B	487 (Broad)	560	1945	(38)
iNOS _{FL} + L-Arg + H4B	512	567	1906	(38)
nNOS _{oxy} + L-Arg	502	565	1932	(42)
nNOS _{oxy} + L-Arg + H4B	502	565	N.D.	(42)
nNOS _{FL} + H4B	498 (Broad)	562	1936	(28,70)
nNOS _{FL} + L-Arg + H4B	503	565	1929	(70)
nNOS _{FL} + L-NOHA + H4B	502	563	1928	(70)
eNOS _{FL} + L-Arg + H4B	512	567	N.D.	(38)

Table II: Listing of the $\nu_{\text{Fe-NO}}$ and $\delta_{\text{Fe-NO}}$ modes of the NO-bound ferric complexes of iNOS_{oxy}, nNOS_{oxy} and full length nNOS (nNOS_{FL})

Complex (Fe ⁺³ -NO)	$\nu_{\text{Fe-NO}}$ (cm ⁻¹)	$\delta_{\text{Fe-NO}}$ (cm ⁻¹)	Ref
iNOS _{oxy}	537 (4) ^a	-	This work.
iNOS _{oxy} + L-Arg	537 (4) ^a	-	This work.
iNOS _{oxy} + H4B	542 (?)	550 (?)	This work.
iNOS _{oxy} + L-Arg + H4B	-	545 (8) ^a	This work.
nNOS _{oxy}	535 (3) ^a		(47)
nNOS _{oxy} + L-Arg	N.D.		
nNOS _{oxy} + H4B	542 (5) ^a		(47)
nNOS _{oxy} + L-Arg + H4B	-	546 (10) ^a	(47)
nNOS _{FL} + H4B	540 (16) ^b		(48)

a. Isotopic shift for ¹⁵N¹⁶O

b. Isotopic shift for ¹⁵N¹⁸O

Table III: Listing of the $\nu_{\text{Fe-NO}}$ and $\delta_{\text{Fe-NO}}$ modes of the NO-bound ferrous complexes of iNOS_{oxy}, nNOS_{oxy} and full length nNOS (nNOS_{FL})

Complex (Fe ⁺² -NO)	$\nu_{\text{Fe-NO}}$ (cm ⁻¹)	$\delta_{\text{Fe-NO}}$ (cm ⁻¹)	Ref
iNOS _{oxy}	N.D.	N.D.	This work.
iNOS _{oxy} + L-Arg	540	-	This work.
iNOS _{oxy} + H4B	N.D.	N.D.	This work.
iNOS _{oxy} + L-Arg + H4B	549 (16) ^a	-	This work.
nNOS _{oxy}	N.D.	N.D.	
nNOS _{oxy} + H4B	543 (15) ^a	-	(47)
nNOS _{oxy} + L-Arg + H4B	549 (15) ^a	-	(47)
nNOS _{FL} + L-Arg	N.D.	N.D.	
nNOS _{FL} + H4B	536	-	(48)
nNOS _{FL} + L-Arg + H4B	549	-	(48)
nNOS _{FL} + H4B	N.D.	N.D.	

a. Isotopic shift for ¹⁵N¹⁶O

Table IV. Calculated heme out-of-plane distortion in various derivatives of eNOS_{oxy} and iNOS_{oxy} based on the NSD analysis.

PDB	Complexes	Doop	B2u	B1u	A2u	Ref
1FOL	eNOS ⁺² + L-Arg	0.97	0.65	0.60	0.36	(58)
1FOO	eNOS ⁺² -NO + L-Arg	0.77	0.42	0.60	0.21	(58)
1FOP	eNOS ⁺² -NO + L-Arg + H4B	1.00	0.68	0.66	0.24	(58)
1NOD	iNOS ⁺³ ($\delta 65$) + L-Arg + H4B	0.83	0.53	0.57	0.26	(8)
1N2N	iNOS ⁺³ -CN ⁻ + L-Arg + H4B	1.08	0.79	0.59	0.41	(59)
1NOS	iNOS ⁺³ ($\delta 114$) + Imidazole	0.71	0.02	0.68	0.17	(9)

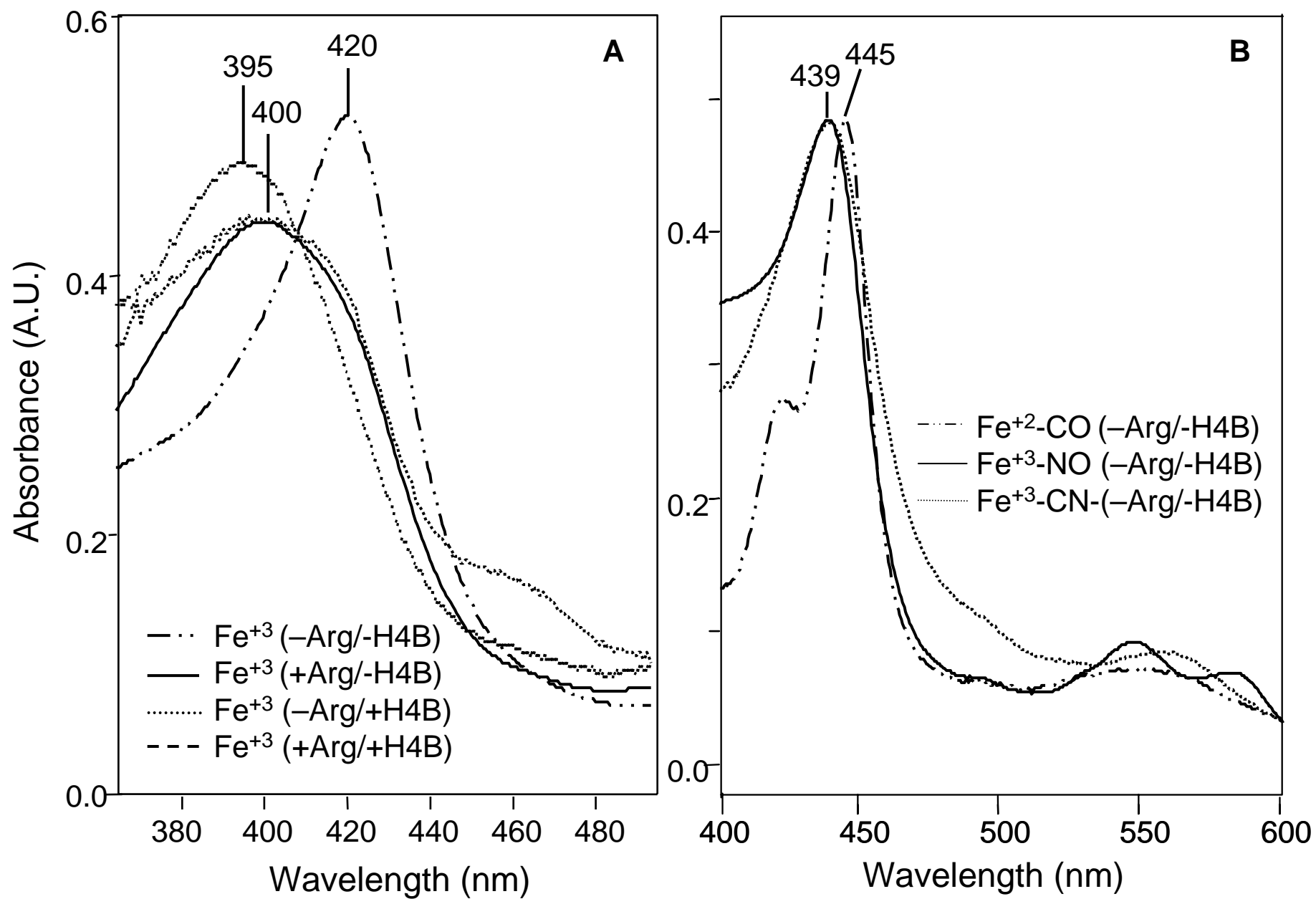


Fig. 1

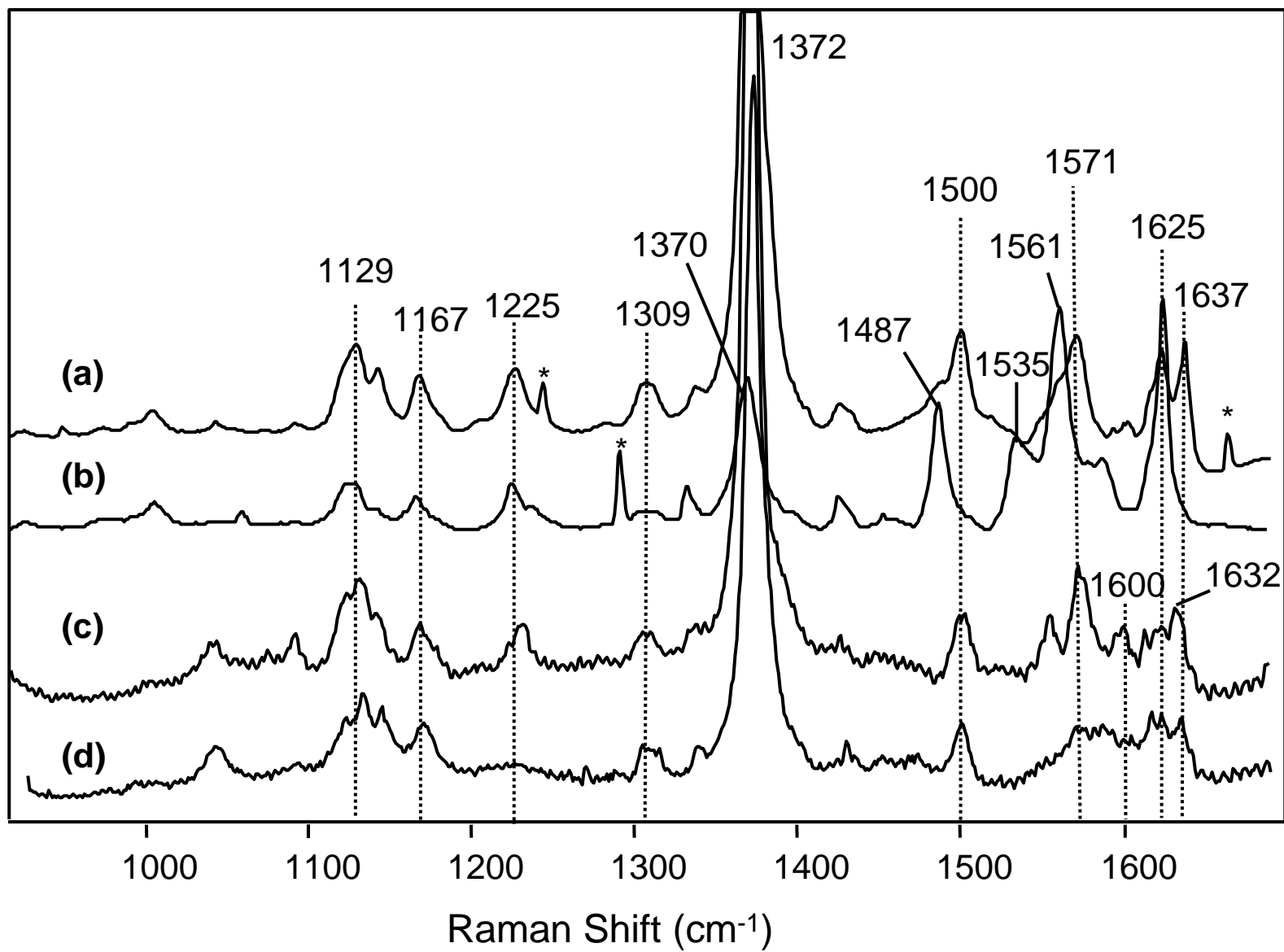


Fig. 2

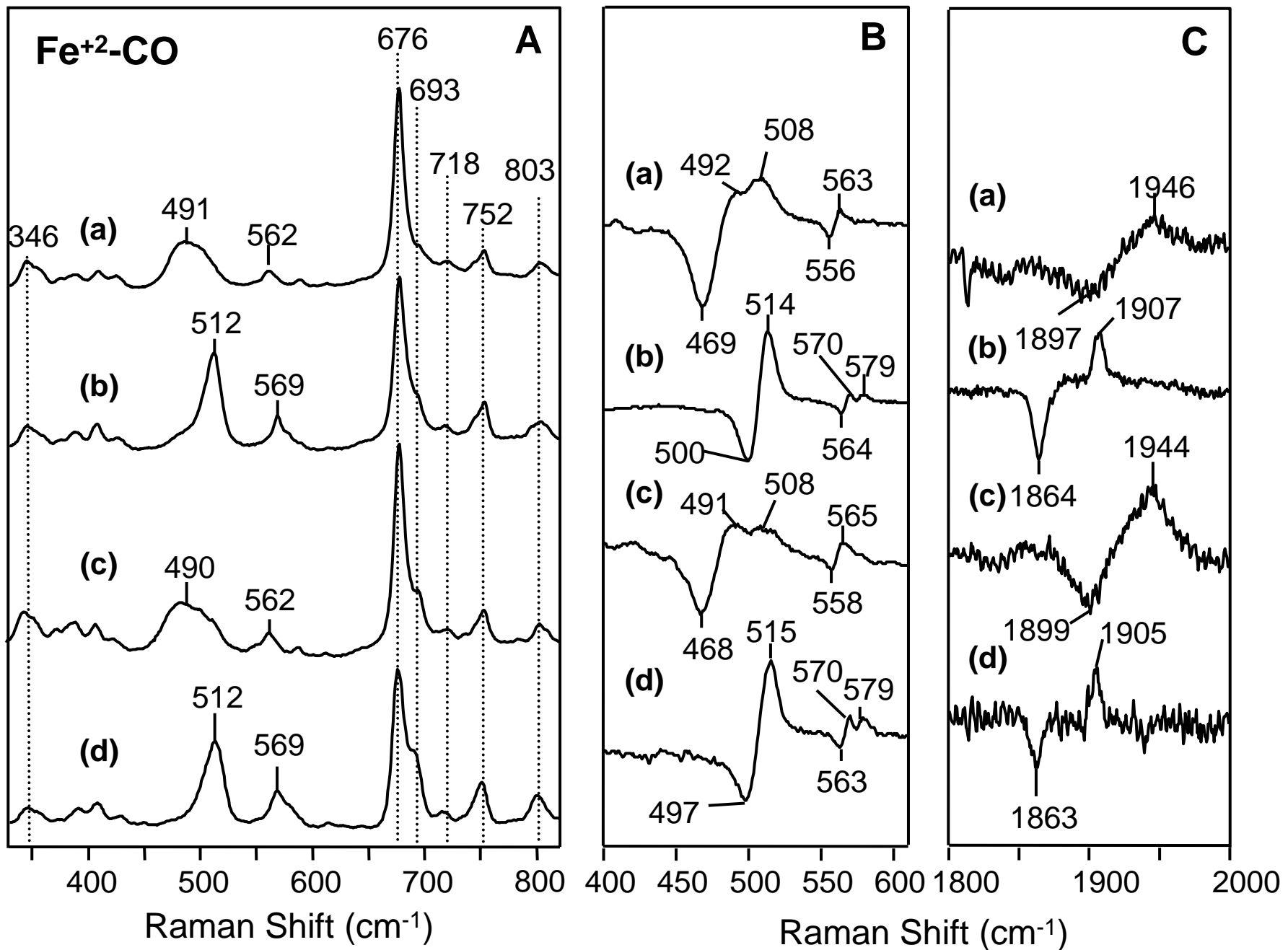


Fig. 3

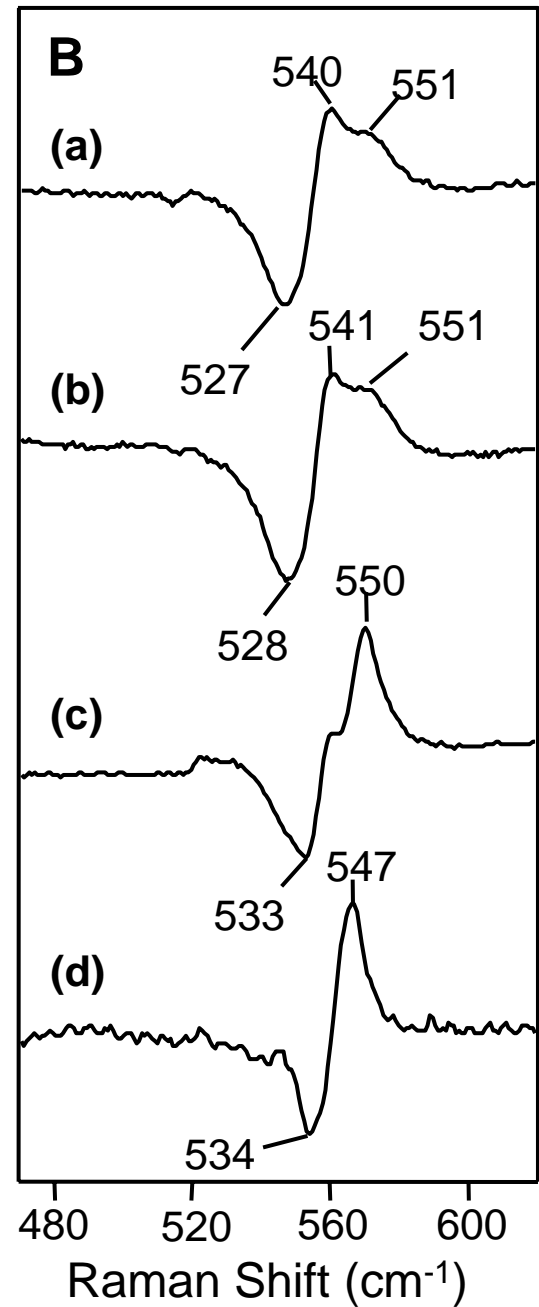
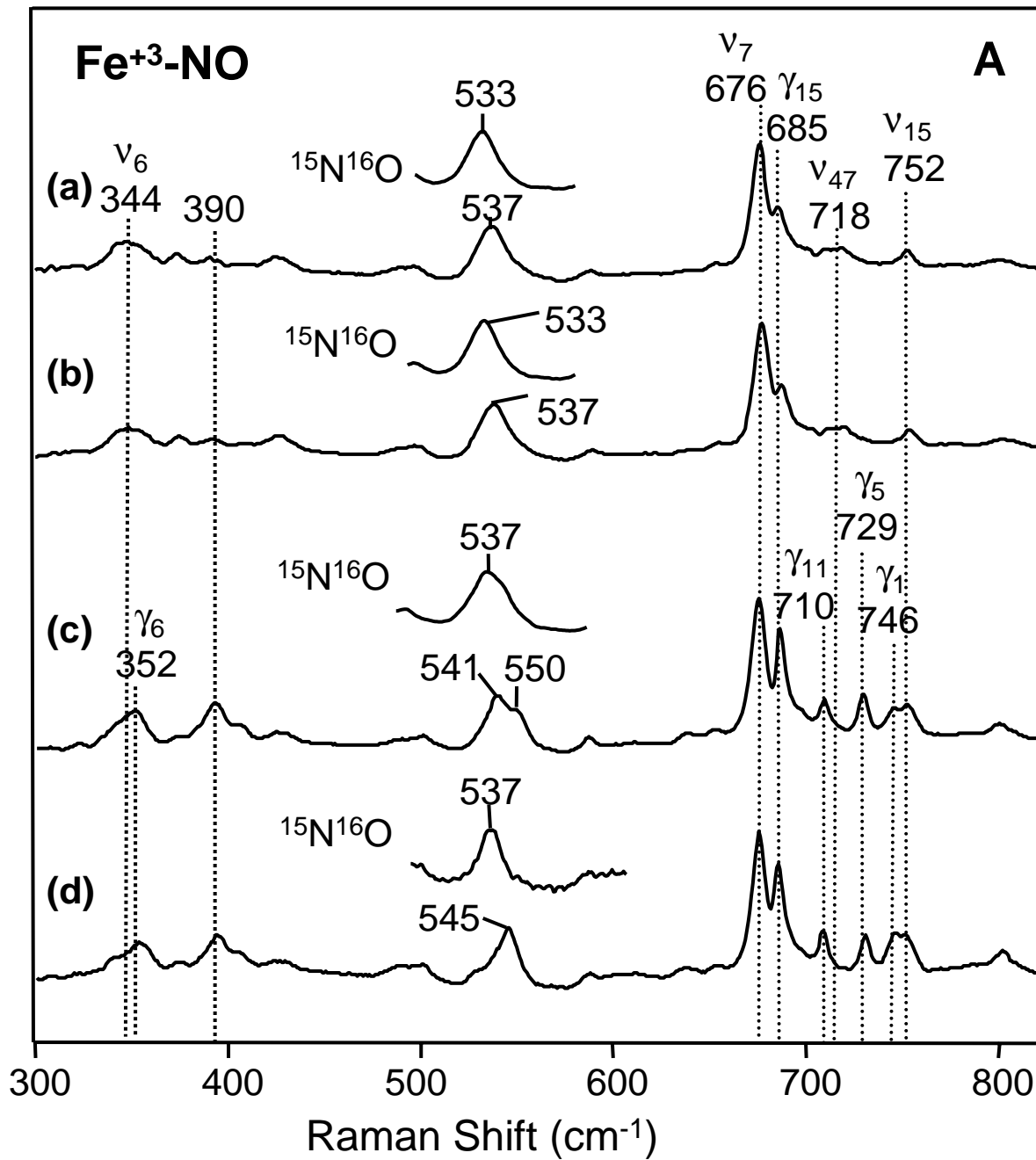


Fig. 4

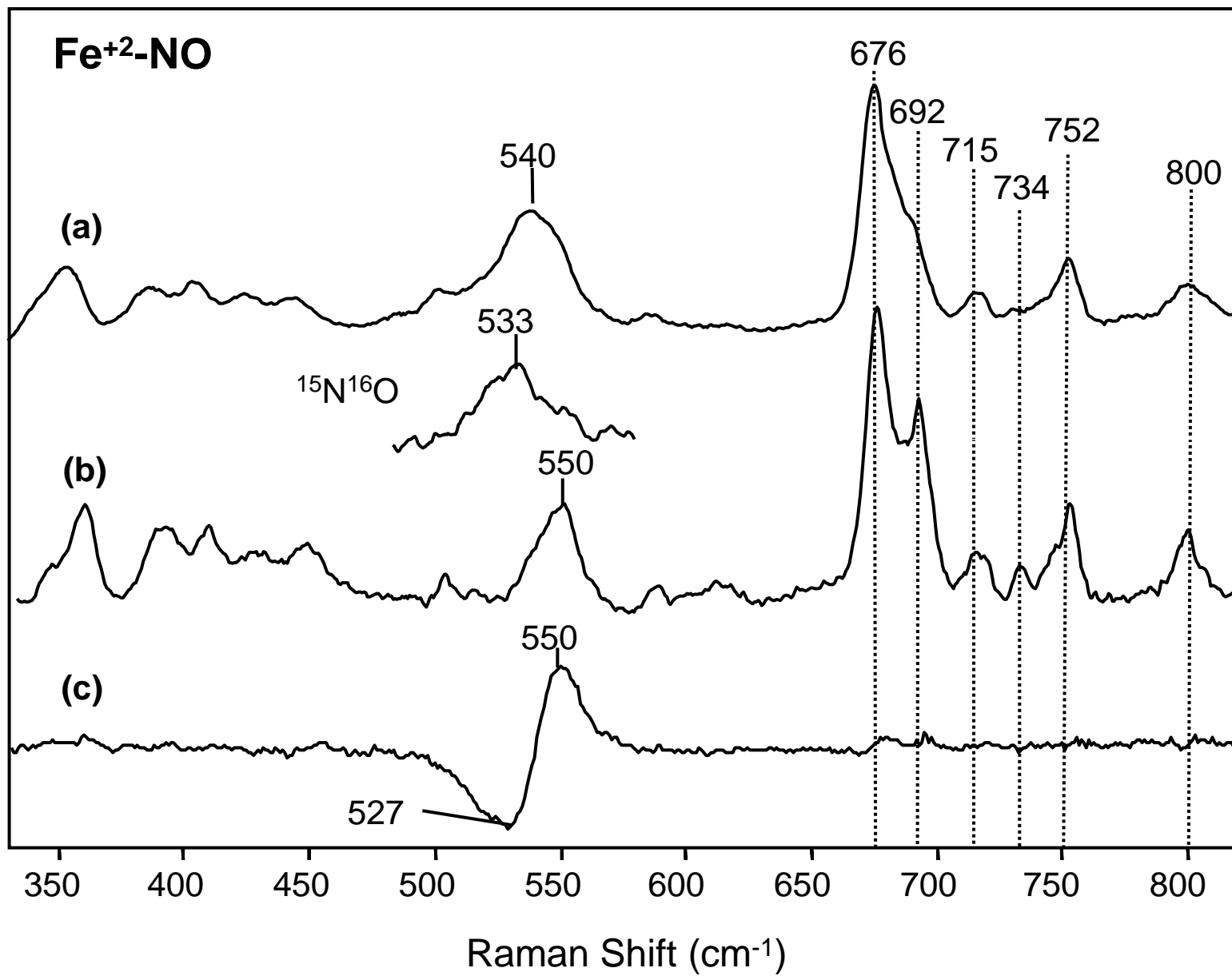


Fig. 5

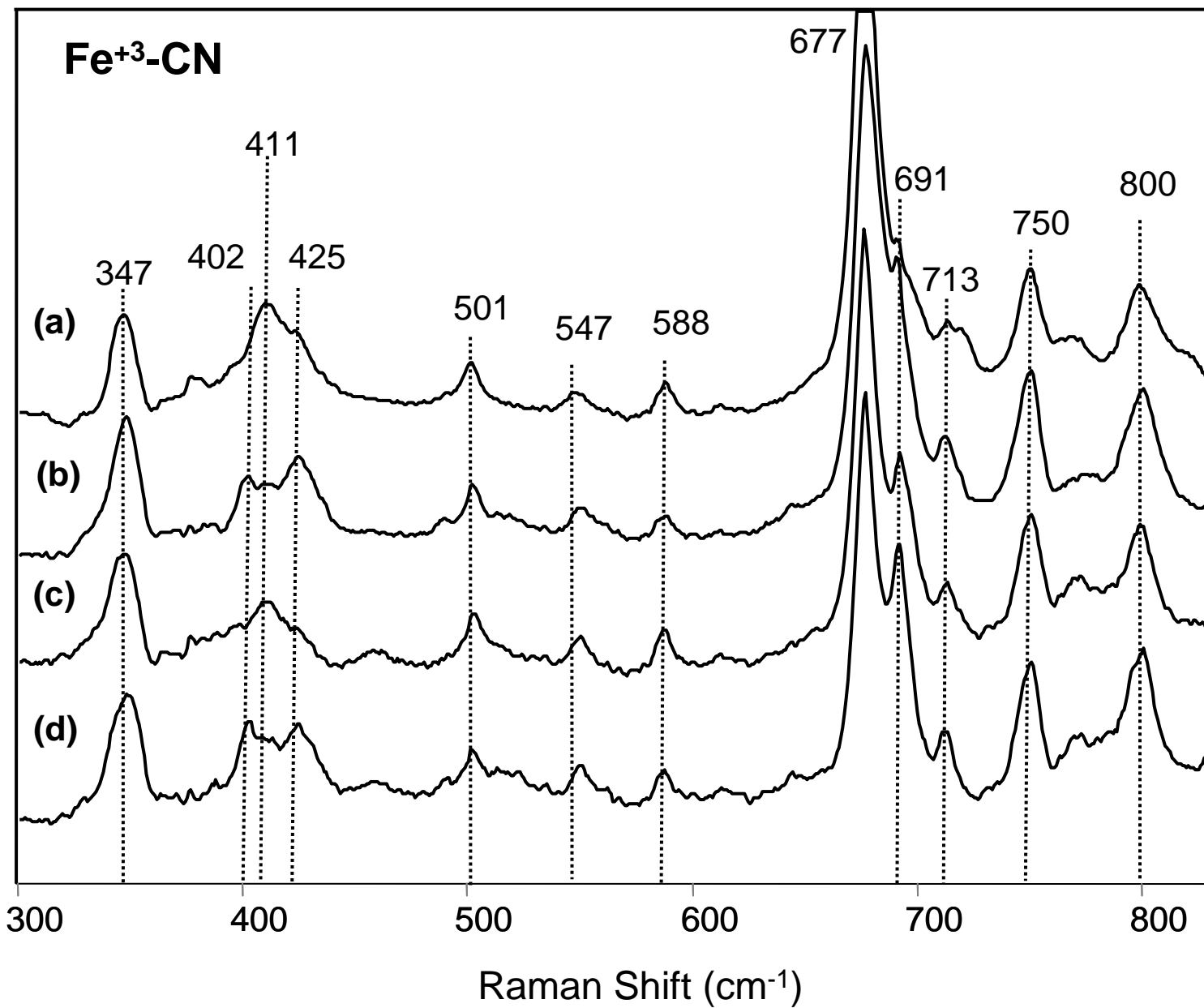


Fig. 6

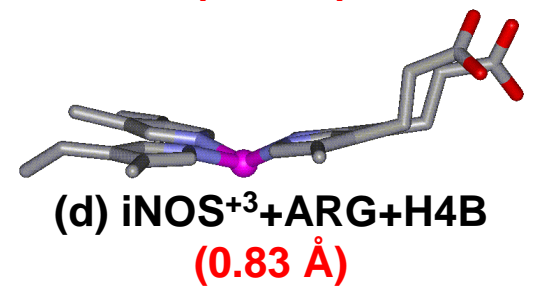
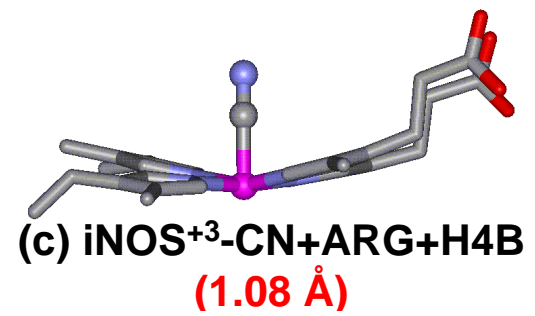
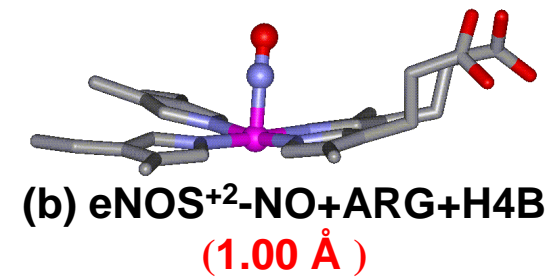
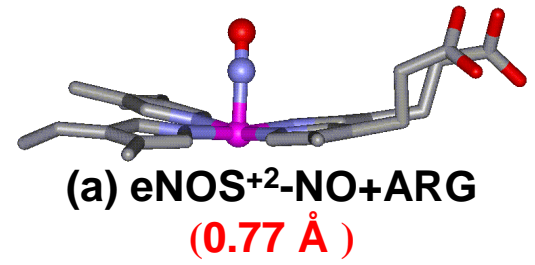
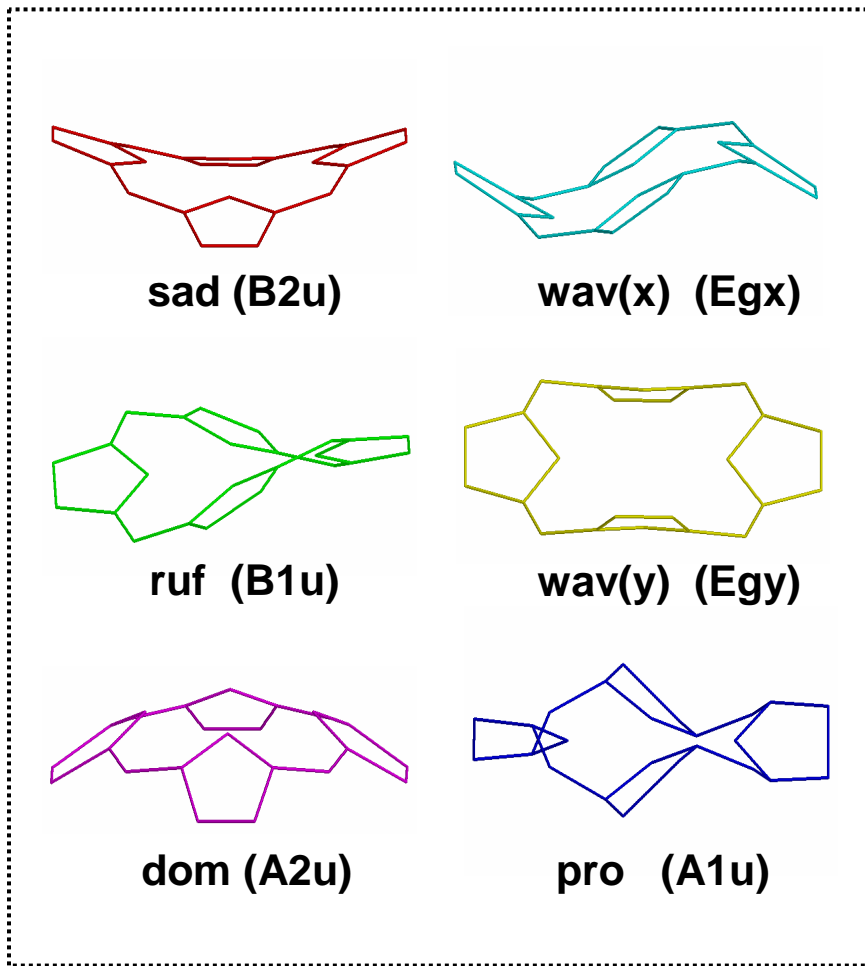


Fig. 7